Copyright Warning & Restrictions

The copyright law of the United States (Title 17, United States Code) governs the making of photocopies or other reproductions of copyrighted material.

Under certain conditions specified in the law, libraries and archives are authorized to furnish a photocopy or other reproduction. One of these specified conditions is that the photocopy or reproduction is not to be "used for any purpose other than private study, scholarship, or research." If a, user makes a request for, or later uses, a photocopy or reproduction for purposes in excess of "fair use" that user may be liable for copyright infringement,

This institution reserves the right to refuse to accept a copying order if, in its judgment, fulfillment of the order would involve violation of copyright law.

Please Note: The author retains the copyright while the New Jersey Institute of Technology reserves the right to distribute this thesis or dissertation

Printing note: If you do not wish to print this page, then select "Pages from: first page # to: last page #" on the print dialog screen

ABSTRACT

MODULATION OF CEREBELLAR PURKINJE CELL ACTIVITY WITH LOW INTENSITY ELECTRIC AND ULTRASOUND STIMULATION

by
Ahmet S. Asan

Non-invasive brain stimulation (NIBS) techniques garner significant interest due to their potential to offer instantaneous and region-specific treatments to neurological disorders. The cerebellum is one of the target sites for NIBS methods due to its central role in motor and cognitive functions. Among several modulation techniques, transcranial electric stimulations (tEs), in particular, transcranial direct and alternating current stimulations (tDCs/tACs), and low intensity focused ultrasound stimulation (LIFUS) show encouraging outcomes in clinical applications. tDCs and tACs are favored due to their low cost and accessibility while LIFUS offers high spatial resolution and deeper penetration without affecting the surrounding structures. In order to better understand the underlying mechanism of these methods in the cerebellum, animal studies are needed since these experiments require invasive surgeries. The goal of this study is to investigate the response of cerebellar PCs to electric and ultrasound stimulation in an animal model.

The first objective is to measure the electric field (e-field) distribution inside the brain parenchyma since e-field is the main parameter that determines the local effects of electrical stimulation. The results of this part show that e-field decays exponentially through horizontal and vertical directions from the stimulating electrode and scattered by the skin up to 80%. Then, tACS and tDCS are applied to the cerebellar cortex respectively while recording the extracellular spike activity from the cerebellar PCs.

The activity of PCs is important because they generate the sole output from the cerebellar cortex, which in turn modifies the output of the deep cerebellar nuclei (DCN). The results of this part demonstrate that the direction of e-field is highly correlated with the level of modulation measured on the PCs. Applying the e-field parallel to the dendritic tree of the PCs generates the highest modulation level. Our data show that PCs have a characteristic response to both DC and AC fields, including entrainment of the simple spike activity at high frequencies. Our findings for the LIFUS also show that spike timing of PCs is strongly entrained with the pulsed ultrasound stimulation, and the level of the entrainment is inversely correlated with the pulse width.

In summary, the low intensity electric and ultrasound stimulation are able to effectively modulate the PC activity in the cerebellar cortex. This warrants research to further look into the mechanism of tES and LIFUS acting on the cerebellar cortex at the cellular level.

MODULATION OF CEREBELLAR PURKINJE CELL ACTIVITY WITH LOW INTENSITY ELECTRIC AND ULTRASOUND STIMULATION

by
Ahmet S. Asan

A Dissertation
Submitted to the Faculty of
New Jersey Institute of Technology
and Rutgers University Biomedical and Health Sciences – Newark
in Partial Fulfillment of the Requirements for the Degree of
Doctor of Philosophy in Biomedical Engineering

Department of Biomedical Engineering

May 2020

APPROVAL PAGE

MODULATION OF CEREBELLAR PURKINJE CELL ACTIVITY WITH LOW INTENSITY ELECTRIC AND ULTRASOUND STIMULATION

Ahmet S. Asan

Dr. Mesut Sahin, Dissertation Advisor — Date
Professor of Biomedical Engineering, New Jersey Institute of Technology

---

Dr. Eric J. Lang, Committee Member — Date
Associate Professor of Neuroscience and Physiology, New York University

---

Dr. Sergei Adamovich, Committee Member — Date
Professor of Biomedical Engineering, New Jersey Institute of Technology

---

Dr. Bart Krekelberg, Committee Member — Date
Professor of Neuroscience, Rutgers University, Newark

Dr. Gail Forrest, Committee Member — Date
Associate Professor of Physical Medicine & Rehabilitation, Rutgers University, Newark

BIOGRAPHICAL SKETCH

Author: Ahmet S. Asan

Degree: Doctor of Philosophy

Date: May 2020

Undergraduate and Graduate Education:

- Doctor of Philosophy in Biomedical Engineering,
  New Jersey Institute of Technology, Newark, NJ, 2020

- Master of Science in Biomedical Engineering,
  New Jersey Institute of Technology, Newark, NJ, 2016

- Bachelor of Science in Mechatronics Engineering,
  Kocaeli University, Kocaeli, Turkey, 2012

Major: Biomedical Engineering

Presentations and Publications:

Asan, A. S., Lang E. J., Sahin M., Entrainment of Cerebellar Purkinje Cells with Directional AC Electric Fields. Submitted for Publication, 2020.

Asan, A. S., Gok S., Sahin M., Electrical Fields Induced Inside the Rat Brain with Skin, Skull, and Dural Placements of the Current Injection Electrode, Published in Plos One, 2019.

Asan, A. S., Sahin M., Modulation of Multiunit Spike Activity by Transcranial AC Stimulation (tACS) in the Rat Cerebellar Cortex, Published in IEEE Engineering in Medicine and Biology Conference, 2019.

Asan, A. S., Sahin M., Modulation of Cerebellar Purkinje Cell Spontaneous Activity with Alternating Currents In the Rat, Published Abstract in Biomedical Engineering Society (BMES) Conference, 2019.

Ordek G., Asan A. S., Cetinkaya E., Skotak M., Kakulavrapu V., Chandra N., Sahin M., Electrophysiological Correlates of Blast-waves Induced Cerebellar Injury, Published in Nature Scientific Report, 2018.

Asan, A. S., Gok S., Sahin M., Electric Fields Induced by Transcutaneous and Intracranial Current Injections in the Rat Brain, Published in IEEE Engineering in Medicine and Biology Conference, 2018.

Asan, A. S., Ordek G., Cetinkaya E., Skotak M., Kakulavarapu V. R., Chandra N. & Sahin M., Assessment of Cerebellar Injury in Rats Using Evoked Potentials and a Behavioral Task, Published Abstract in Biomedical Engineering Society Conference, 2017.

To my beloved parents
(Sevgili Annem ve Babama)

ACKNOWLEDGMENT

First and foremost, I would like to express my sincere gratitude to my advisor Dr. Mesut Sahin. This work would not have been possible without his guidance, support, and encouragement.

I would also like to thank Dr. Eric J. Lang, Dr. Sergei Adamovich, Dr. Bart Krekelberg, and Dr. Gail Forrest for serving in my dissertation committee and their valuable contributions to my research.

A special thank you to all Neural Prosthetics Lab members and my friends for their help and support.

Above all, I am forever indebted to my parents, Murat and Rahime, and my sisters, Esra and Sedanur for their encouragement and devotion. I will never be able to compensate for your support and sacrifices.

TABLE OF CONTENTS

TABLE OF CONTENTS
(Continued)

Chapter **Page**

TABLE OF CONTENTS
(Continued)

Chapter **Page**

LIST OF FIGURES

CHAPTER 1

INTRODUCTION

1.1 Neuromodulation and Cerebellar Anatomy

Neuromodulation technology acts on nerves and changes their activity by delivering electrical or pharmaceutical agents (Henry, Deckert, Guruviah, & Schmidt, 2016). This technology is used to improve the patient's quality of life who suffers from severe chronic illnesses. Unlike pharmaceutical agents, stimulation techniques can locally intervene the neural activities and provide treatment to many neurological diseases such as Parkinson's disease, essential tremor, chronic pain, and epilepsy (Moreines, McClintock, & Holtzheimer, 2011). This technology has also become a key treatment option for neuropsychiatry conditions including management of severe depression (Lipsman et al., 2014), and obsessive compulsive disorders (Bais, Figee, & Denys, 2014). The selection of the neuromodulation modality for medical applications is decided based upon the location, the size of targeted regions, and the desired impact. More recently, low intensity focused ultrasound stimulation (LIFUS) has also come into prominence due to offering a higher spatial resolution and deeper penetration (Bystritsky et al., 2011).

Traditionally, the cerebellum was thought to be involved in only motor functions and fine movements. However, studies over the past decades revealed the crucial role of the cerebellum on cognition such as language processing (Booth, Wood, Lu, Houk, & Bitan, 2007) and visuospatial attention (Yamaguchi, Tsuchiya, & Kobayashi, 1998). The cerebellum consists of 80% of the neurons in the brain while constituting 10% of the entire volume with its stereotypical circuitry (Herculano-Houzel, 2009). There are only two

inputs entering the cerebellar cortex, climbing fibers (CF) and mossy fibers (MF). Mossy fibers mainly arise from pontine nuclei and synapse onto granule cells in the granule cell layer. Granule cell axons, also called parallel fibers, ascend to molecular layer, bifurcate and synapse onto Purkinje cells (PCs), which generate the simple spike as a result. On the other hand, CFs arise from inferior olive and terminate directly on the PCs. CFs connection on the PCs results in the complex spike generation.

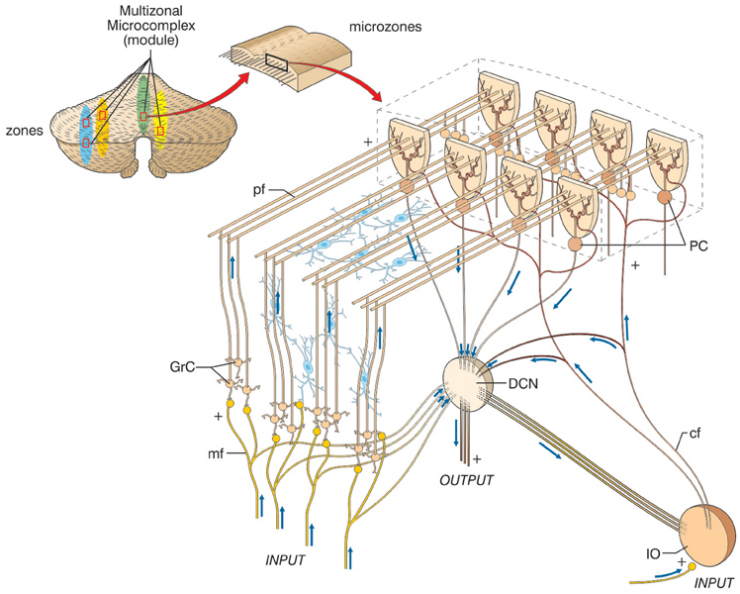

Figure 1.1 The circuitry in the cerebellar cortex.
Source: D'Angelo, E. and S. Casali, *Seeking a unified framework for cerebellar function and dysfunction: from circuit operations to cognition.* Frontiers in Neural Circuits, 2013. **6**(116) (D'Angelo & Casali, 2013).

Spatiotemporal pattern of simple and complex spike activity is essential for generation of a meaningful output from the cerebellar cortex (De Zeeuw et al., 2011). Simple spike and complex spike synchrony of the PCs that project onto the same deep cerebellar nuclei (DCN) is likely to shape and determine the cerebellar output by adjusting the timing and firing rate of the DCNs (A. Person & Raman, 2012; Tang, Suh, Blenkinsop, & Lang, 2016). Multiple studies have shown that synchrony of the PCs is significantly

improved during the execution of a cerebellar dependent movement. Therefore, damage on this circuitry causes several impairments such as ataxia, postural instability, tremor, impairments in balance and fine motor skills, and cognitive deficits (Schmahmann, 2004). In this respect, neuromodulation techniques offer alternative window of opportunities as a therapeutic approach to intervene the cerebellar circuitry.

1.2 Transcranial Electric Stimulation (tES)

Non-invasive brain stimulation techniques target neuronal structures and modulate their activity. Among these methods, tES, in particular tDCS and tACS, are reporting encouraging outcomes in clinical research (Dedoncker, Brunoni, Baeken, & Vanderhasselt, 2016; Schutter & Wischnewski, 2016). tDCS utilizes direct currents while tACs injects biphasic currents and reverses the electron stream periodically. Both tDCS and tACS use weak currents and expectedly cause subthreshold modulation at the cellular level. Although the underlying mechanism of these methods still remains as an active area of research, it appears that, in addition to shifting the resting membrane potential, the applied electric field can also manipulate the neurotransmitter concentration in the microenvironment (M. A. Nitsche & Paulus, 2000a; Stagg, Best, Stephenson, O'Shea, et al., 2009).

1.2.1 Transcranial Direct Current Stimulation (tDCS)

tDCS comes into prominence due to its cheap price tag and accessibility as well as its ability to modulate neuronal function without causing any significant discomfort to the patients (Marom Bikson et al., 2016b). In a seminal work published in 1963, Bindman *et al.* showed that intra-cortical direct current stimulation of the brain changed the spontaneous firings of sensorimotor cortex neurons in anesthetized rats (L. J. Bindman, O.

C. Lippold, & J. W. Redfearn, 1964). The cortex activity was diminished during the cathodal stimulation but increased during the anodal stimulation. More recent studies on rats (Marom Bikson et al., 2016a), cats (Schweid, Rushmore, & Valero-Cabré, 2008), and humans (M. A. Nitsche & Paulus, 2000b) reported similar effects when the current was applied transcranially.

Transcranial direct current stimulation utilizes low intensity electrical currents to modulate the neural activity both via excitation and inhibition. However, the exact cellular and molecular mechanisms underlying the tDCS remain unknown. According to one plausible theory supported by the studies of Nische *et al*. (Michael A. Nitsche et al., 2003) and Purpura and McMurtry (Purpura & McMurtry, 1965) , tDCS alters the resting potential of the neuronal cell membrane and the synaptic microenvironment causing excitability changes in the cortical neurons. As for the after-effects of tDCS (Roche, Geiger, & Bussel, 2015) , it has been suggested that GABA concentration decreases after anodal stimulation with no change in the glutamate levels, whereas both decline after cathodic stimulation (Stagg, Best, Stephenson, Shea, et al., 2009) . Based on this theory, tDCS induced plasticity can be explained by the changes in the availability of these two most common neurotransmitters in the CNS.

Recent studies demonstrated that neuronal excitation and inhibition are not determined by the stimulating current direction per se (anodal vs. cathodal), but also by the position and orientation of the neuronal structures relative to the electric field. Based on rat hippocampal slice experiments, Kabakov *et al*. showed that axonal orientation determined the net effect of the DC field and dendritic orientation had an impact on the magnitude (Kabakov, Muller, Pascual-Leone, Jensen, & Rotenberg, 2012). Bikson *et al*.

applied uniform DC electric fields on CA1 neurons and concluded that the polarization varied along the somato-dendritic axis and dendritic depolarization was sufficient to induce firing even when the soma was in a hyperpolarizing zone (Bikson et al., 2004b). In another study (Radman, Ramos, Brumberg, & Bikson, 2009b), authors predicted that if optimally oriented, the soma of a layer V pyramidal cell is the most sensitive cellular compartment to polarization under weak electric fields. The results of these highly controlled *in vitro* studies are supported by computational studies (Datta, Bikson, & Fregni, 2010) (Opitz, Paulus, Will, Antunes, & Thielscher, 2015), which caution the tDCS researchers to pay closer attention to electric field distributions inside the brain.

1.2.2 Transcranial Alternating Current Stimulation (tACS)

Brain oscillations carry important information for cognitive functions (Knyazev, 2007) and aberration of these oscillations causes various mental disorders (Buzsáki & Draguhn, 2004). Modulation of these rhythmic activities offers treatment options to those who suffer from mental difficulties such as depression (Fitzgerald & Watson, 2018) and attention deficit (Lenartowicz, Mazaheri, Jensen, & Loo, 2018). Several studies have shown that the alternating current stimulation is able to synchronize intrinsic neural activities and entrain the endogenous oscillations. Frochlich *et al*. demonstrated that directing the weak sinusoidal current to a cortical slice preparation was able to provoke neural spikes and ultimately modify the multiunit activity (Fröhlich & McCormick, 2010). Zaehle *et al*. also showed that tACS enhances the alpha oscillation and its effect continues after the end of stimulation (Zaehle, Rach, & Herrmann, 2010). Several other studies also reported the long-lasting effect of tACS (Kasten, Dowsett, & Herrmann, 2016; Vossen, Gross, & Thut, 2015) thus suggesting neuroplasticity. The change on the spike activity and phase shift led

by tACS are considered to be the mechanism behind the plasticity observed (Herrmann, Rach, Neuling, & Strüber, 2013; Vossen et al., 2015).

There has not been extensive research looking at the effect of tACS on the cerebellar circuitry. Naro *et al*. also applied tACS over the right cerebellar hemisphere at 10, 50, 300Hz and measured their effects on the motor evoked potentials (MEP). Their findings show that while 50 Hz tACs increases the MEP, 10 and 300 Hz-tACS cause mild or no effect on the MEP (Naro et al., 2016a).

1.3 Focused Ultrasound Stimulation (FUS)

Ultrasound is acoustic waves with frequencies higher than 20kHz. In 1929, Harvey *et al*. showed that ultrasound can irreversibly excite nerves and muscle tissues in frogs and turtles (Harvey, 1929). In later studies, Fry *et al*. demonstrated that high intensity ultrasound can be used to ablate brain tissue (W. J. Fry, Fry, Barnard, Krumins, & Brennan, 1955; W. J. Fry, Mosberg, Barnard, & Fry, 1954). Fry also showed that targeting the lateral geniculate nucleus with ultrasound inhibits the electrical potential in the visual cortex (F. J. Fry, Ades, & Fry, 1958). There are several early scientific studies demonstrate US nerves stimulation. Recent studies also indicate low intensity ultrasound has a reversible effect on nerves and it can inhibit and excite the neurons. Tufail *et al*. showed reversible excitation during LIFUS on rat's motor cortex(Tufail et al., 2010). The ultrasound effect is divided into thermal and nonthermal effect regarding the intensity level. High intensity ultrasound causes the heating and cavitation on the tissue called thermal effect. Even though heating is capable of increasing excitability of the neurons, it decreases synaptic transmission and tissue homogenization also results in protein denaturation, and DNA fragmentation

(Rezayat & Toostani, 2016). The non-thermal effect is produced by low intensity ultrasound stimulation (LIFUS) and it has no known side effects on the region of interest (Bystritsky et al., 2011). The advantages of the LIFU over the other stimulation modalities are, first of all, it is a non-invasive technique, unlike DBS. It is region specific which is capable of focusing region of interest with 1mm precision. Unlike TMS and tDCs, this technique can aim at deeper brain regions.

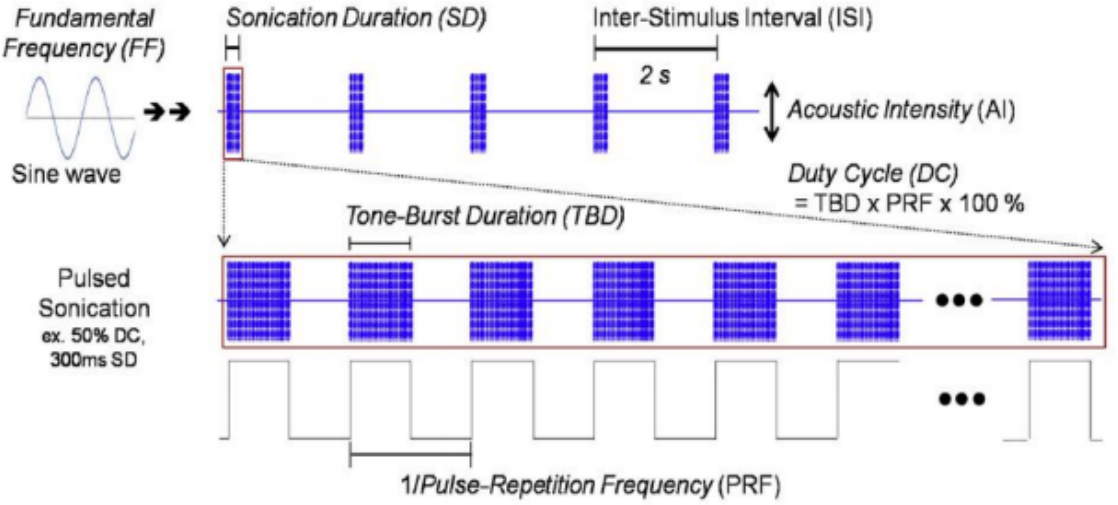

Figure 1.2 Definition of sonication parameters controlled by a function generator.
Source: Lee, W., *et al*., Image-Guided *Transcranial Focused Ultrasound Stimulates Primary Somatosensory Cortex*. Scientific Reports, 2015. 5(1): p. 8743 (Lee et al., 2015).

The US train parameters determine the effect of ultrasound stimulation. These parameters are center frequency (CF), tone burst duration (TBD), pulse repetition frequency (PRF), acoustic intensity (AI), sonication duration (SD), and duty factor (DF) (King, Brown, Newsome, & Pauly, 2013). Yuan *et al*. showed that increasing the AI leads producing higher EPs response from the rat hippocampus (Yuan, Yan, Ma, & Li, 2016). Yoo *et al*. also demonstrated TBD and PRF define the stimulation type, excitatory or inhibitory (Yoo et al., 2011). The underlying mechanism of the ultrasound stimulation on

nerves is not entirely understood. One possible mechanism is that ultrasound may mechanically stretch the nerves' membrane. Stretched membrane lipid bilayers, membrane proteins, and extracellular proteins lead to membrane depolarization (Tyler, 2012). Also, voltage-gated ion channels and neurotransmitter receptors have mechanosensitive sensors and that make them the potential targets for ultrasound (Tyler et al., 2008b). Alternative studies suggest that US stimulates neural circuitry by increasing the activity of microtubules, which have a high resonance frequency (Hameroff et al., 2013).

CHAPTER 2

ELECTRICAL FIELDS INDUCED INSIDE THE RAT BRAIN WITH SKIN, SKULL, AND DURAL PLACEMENTS OF THE CURRENT INJECTION ELECTRODE

2.1 Objective / Background Information

Transcranial electrical stimulation (tES) has emerged as an effective non-invasive technique for modulation of the brain activity in recent years, while the earliest studies date back more than a century (Priori, 2003). In general, the safety of tES and its derivations has now been agreed upon so long as the current is kept below 2mA, although recent reports seem to suggest 4mA as the limit (Chhatbar et al., 2017). These tES derivations include transcranial direct current stimulation (tDCS), transcranial alternating current stimulation (tACS), and transcranial random noise stimulation (tRNS) (Antal, Alekseichuk, Bikson, Brockmöller, et al., 2017; Marom Bikson et al., 2016a). Despite widespread interest in clinical applications, the exact mechanisms of action for tES are still being investigated.

Aforementioned tES techniques inject weak electrical currents through the brain and presumably cause only subthreshold modulation of the neuronal membrane potentials (Woods et al., 2016). Early animal studies demonstrated that neuronal firing rates could be modulated by applying direct currents (DC) to the brain (L. J. Bindman, O. C. J. Lippold, & J. W. T. Redfearn, 1964; Creutzfeldt, Fromm, & Kapp, 1962) and the modulatory effects of transcranial DC electric fields were confirmed in human studies (N. Lang et al., 2005; M. A. Nitsche & Paulus, 2000b). While the excitatory and inhibitory effects of tDCS are attributed to the direction of the applied current on a larger scale (anodal *vs.* cathodal) (Lynn J. Bindman et al., 1964; M. A. Nitsche & Paulus, 2000b; Terzuolo & Bullock, 1956), a more detailed analysis revealed that the primary factor is the position and orientation of

the individual neuronal structures relative to the electric field. *In vitro* measurements on rat hippocampal slices showed that the amplitude and delay of the population spikes evoked by orthodromic stimulation were affected linearly by the applied uniform electric fields (Bikson et al., 2004a). Furthermore, even small electric fields induced polarization of CA1 pyramidal cells of the hippocampus when applied parallel to the somato-dendritic axis but failed to do so when applied perpendicularly. Studies on the rat motor cortex slices indicated that somatic polarization was also correlated with the neuronal morphology, and the layer V pyramidal cells were the most sensitive to subthreshold electric fields (Radman, Ramos, Brumberg, & Bikson, 2009a). In general, it seems that a realistic estimation of the electric field distribution inside the brain parenchyma is needed as a starting point for accurate interpretations of the neurological impact of the intervention.

The electric field can be controlled by adjusting the stimulation current/charge intensity and steered to a certain extent by careful positioning of the extracranial electrodes. Nevertheless, the electrical properties of different tissues that the current passes through play a significant role in distribution of the electric field. Direct in vivo measurement of the electric field in human subjects is not an option from a clinical standpoint, thus most investigators resort to computational models in order to approximate the electric field distribution in the human brain under varying stimulation intensities and electrode arrangements. Miranda *et al*. used a spherical head model and estimated that almost 50% of the injected current is shunted through the scalp (Miranda, Lomarev, & Hallett, 2006). Datta *et al*. used a more advanced head model where gyri/sulci specificity was defined and predicted that the electric field was concentrated at distinct sites, like the walls of the gyri (Datta et al., 2009). In summary, tES induced current flow is influenced by several factors

including: 1) skull and scalp thicknesses and their compositions, 2) CSF thickness and conductivity, 3) gyri/sulci morphology, 4) electrode size and geometry, and 5) positioning of the stimulating and return electrodes (Datta et al., 2009; Opitz et al., 2015).

In addition to human computational models, tES effects have been studied in animals where the main interests are understanding the underlying cellular and molecular mechanisms, optimizing stimulation protocols, and establishing safety limits. To this end, animal models provide ample opportunities to rapidly develop new tDCS methodologies and measure the outcomes while manipulating the stimulation parameters within a large range that may not be feasible clinically (see (Jackson et al., 2016) for a review). For accurate interpretation of the results from these animal studies, realistic estimates of the induced electric field distribution are needed. Direct measurement of the electric fields in brain tissue goes back to as early as 1950s with experiments carried on anesthetized monkeys (Hayes, 1950), although not many follow-up studies reported since then. Chan *et al*. conducted a series of experiments using isolated turtle cerebella, and studied the relationship between the applied fields and the spontaneous neuronal activity (Chan, Hounsgaard, & Nicholson, 1988; Chan & Nicholson, 1986). More recent studies on monkeys (Opitz et al., 2016) and rats (Vöröslakos et al., 2018) also reported electric field measurements, although restricted either to the cortical surface or a single horizontal plane, respectively.

The tDCS technique can benefit from *in vivo* animal data, which are clearly lacking in the literature, for better understanding of the mechanisms. While the computational models provide a basic understanding of how electrical currents are distributed through the

animal brain (Gasca et al., 2011) as much as the human brain, they can lead to unrealistic conclusions if they primarily depend on conductivity measurements gathered from ex vivo tissue samples (Huang et al., 2017). Furthermore, anatomical differences in the brain size and the skin, skull, and CSF thicknesses make it difficult to extrapolate the results of an electric field model developed for one species to another. In this study, we used a rat model to measure the intracerebral voltages at varying depths and horizontal distances from the stimulating electrode. Vertical electric fields were reported for three stimulation conditions in which the anodic electrode was placed over the shaved skin, the skull, and the dura mater. The rat brain was selected in this study due to its common usage as an animal model. We anticipate that the results of this study will provide a reference point for more realistic estimations of the electric field distribution in other studies using the rat model and help to improve the reproducibility of the reported tES effects. Some of the results, such as the shunting effect of the skin and the CSF, agree with modeling predictions, while some others such as the relatively smaller attenuation by the rat skull, the E-field peaks at the white/gray matter border, and insensitivity of the field to the reference electrode location are among the practical findings of this study.

2.2 Methods

2.2.1 Animal Surgery

Ten Sprague Dawley rats (250-350g, male) were used in this study for direct measurements of the electric field distribution in the brain parenchyma. This study was carried out in strict accordance with the recommendations in the Guide for the Care and Use of Laboratory Animals of the National Institutes of Health. The protocol was approved by the Institutional

Animal Care and Use Committee (IACUC), Rutgers University, Newark, NJ (Protocol Number: 201702616). Anesthesia was induced with 5% isoflurane gas in an induction chamber, maintained by 1–3% isoflurane in 95% oxygen after moving the animals to a stereotaxic frame, and monitored using the toe pinch reflex. All efforts were made to minimize suffering. Blood oxygen level was monitored via a pulse oximeter (NPB-40, Nellcor Puritan Bennet) from the hind paw. Body temperature was measured with a rectal temperature probe (World Precision Instruments-WPI) and regulated with a heating pad (WPI) underneath the animal over the course of surgery. The hair over the head was shaved with an electric shaver and the skin was treated with a depilatory cream to remove the fine hair. The skin was then cleansed with antiseptic solution.

2.2.2 Current Injection over the Skin

A 1.5mm diameter helical wire electrode was used to inject the electric currents. The helical electrode that is hollow in the center allowed us to make E-field measurements underneath the electrode. In order to make a helical electrode, a Ag/AgCl wire with 125μm uncoated thickness (A-M Systems, #786000) was wrapped around a 1.25mm diameter rod 4 times to form a helix with a large surface area and thus a lower impedance. The impedance was confirmed to be below 10kΩ @1kHz in phosphate buffered saline (PBS, Sigma-Aldrich). The center of the electrode was filled with conductive gel to ensure good contact with the skin and distribute the current more uniformly at the base of the electrode. The helical electrode was placed with its center positioned 2mm lateral (left or right) from the sagittal suture and 2mm either rostral or caudal to the coronal suture. Another Ag/AgCl wire was inserted to the ipsilateral shoulder muscles as the return (cathodic) electrode for the injected current. Ten monophasic anodic pulses were delivered as a train at 100μA amplitude,

100ms pulse width, and a repetition rate of 4Hz. The amplitude was switched to 200μA at times to increase the signal-to-noise ratio where the recorded amplitudes were too small. In this protocol, substituting pulsed stimulation for DC allowed us to overcome the poor DC response of the metal recording electrodes.

A sharp cut was made into the skin with a surgical blade at the edge of the stimulation electrode to expose the skull caudally while leaving the skin underneath the electrode intact (Figure 2.1B). Two 1mm diameter craniotomy holes were drilled 2mm and 4mm away from the caudal edge of the stimulation electrode using a micro drill (OmniDrill 35, WPI). A tungsten electrode (0.5 MΩ, TM33B05H, WPI) was inserted into the craniotomy hole to record the induced voltages as a function of depth with respect to another Ag/AgCl reference electrode attached on the skull near the recording electrode using dental acrylic. The dura was punctured with the sharp tip of the tungsten electrode and the first recording was made at the level of the cortical surface (depth = 0). Using a 10μ-resolution micromanipulator (Kite-R, WPI), the tungsten electrode was advanced into the brain parenchyma in 0.2mm steps until reaching 4mm depth and thereafter in 0.5mm steps up to a depth of 6mm. The procedure was repeated in both craniotomy holes, at 2mm and 4mm horizontal distances from the stimulation electrode. The rising and falling edges of the recorded signals were marked using an automated algorithm in MATLAB (Mathworks Inc.) to quantify the induced voltage amplitudes (see Figure 2.3 inset). In some animals, this procedure was repeated on the contralateral side of the brain to obtain an additional set of measurements.

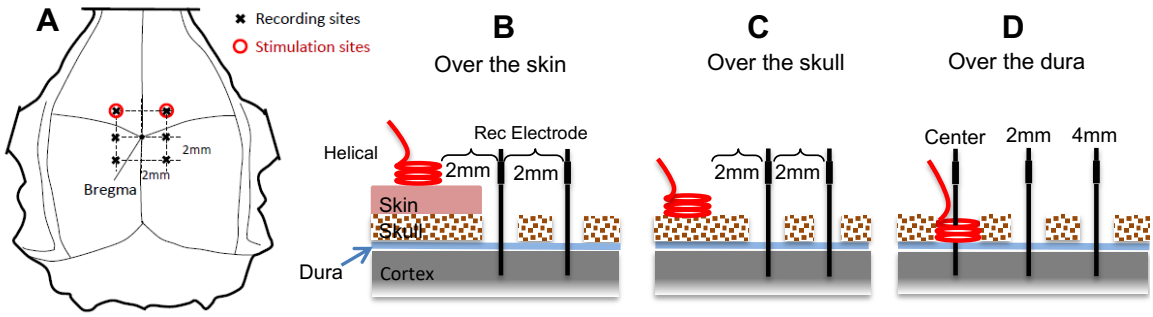

Figure 2.1 Drawings show the three different placements of the stimulation electrode on the rat's head: A) top view. The vertical cross sections of the skin and skull in B, C, and D show the placements of the helical wire stimulation electrode: B) over-the-skin, C) over-the-skull, and D) over-the-dura, and the craniotomy holes for E-field measurements. Tungsten recording electrodes were inserted through the craniotomy holes at center (for over-the-dura stimulation only), and 2mm and 4mm horizontal distances from the stimulation electrode.

2.2.3 Current Injection over the Skull

The skin over the top of the skull was completely removed in this step, mostly in the same animals used above. After removing the periosteum, bone wax was applied to the muscles around the edges and the skull sutures on top to stop bleeding. The stimulation electrode was placed onto the skull (Figure. 2.1C) at the same coordinates used with over-the-skin electrodes measured with respect to the bregma. The voltage measurements were made following the same procedure above with slight repositioning of the tungsten electrode in the same craniotomy holes in order to avoid damaged tissue from the previous penetration.

2.2.4 Current Injection over the Dura

A 2mm craniotomy hole was made at the coordinates of the stimulation electrode to inject the current directly through the dura (Figure 2.1D). A helical wire electrode (1.5mm diam.)

was placed about 0.5mm above the dura mater and anchored to the edge of the skull hole with small amounts of cyanoacrylate glue and the hole was filled with normal saline. The distances between the caudal edge of the helical electrode and recording holes were kept at 2mm and 4mm as before. An additional set of voltage recordings were made by inserting the tungsten electrode through the center of the stimulation electrode.

Finally, in order to investigate the effect of the current return electrode position, the Ag/AgCl wire inserted to the ipsilateral shoulder muscles was moved to the contralateral shoulder, the hind leg, and the submandibular muscles via needle insertions. The voltage measurements were repeated near the cortex and at various depths with the recording electrode in the center of the helical electrode for these four different positioning of the current return electrode for comparison.

2.2.5 Data Collection and Analysis

The signals were collected in a large Faraday cage and first amplified by a gain of 100 (Model 1700, A-M Systems, WA) with filters setting of 10 Hz–10 kHz, and then sampled at 25kHz through a National Instruments data acquisition board (PCI 6071) controlled by custom-designed MATLAB codes. Stimulus-triggered averaging (STA) was used (N = 10) to suppress the background neural activity and other sources of random noise. The averaged signal was further band-pass filtered in MATLAB (10 Hz– 1 kHz) before analyzing. Voltage transitions within 2ms window around the rising edge of the square pulses were taken as the induced voltage at the corresponding depth. The first derivative of the voltage data with respect to depth was computed as the electric field (E-field). All field measurements were made exclusively in the vertical direction (VE-field) in this study. Horizontal E-field measurements would require derivation of the voltage measurements

made through different brain penetrations and lead to large calculation errors due to even slight changes in the absolute value of the voltages measured, which could easily occur from repositioning of the recording reference electrode between penetrations.

2.2.6 Comparison with Theoretical Models

The resistance of a monopolar disk electrode at the surface of a semi-infinite, homogeneous, and isotropic medium was first derived by Newman (Newman, 1966) as a function of the electrode radius (a), and the conductivity of the medium (σ). The potential at the surface is found as $Vo = I/(4\sigma a)$, where I is the electrode current. Wiley and Webster then solved the Laplace's equation for the voltage distribution inside the semi-infinite volume conductor for a similar disk electrode (Wiley & Webster, 1982). By substituting zero for the horizontal axis r in their equation, we find the voltage profile at the electrode center, which starts from Vo at z=0 and declines with increasing values of the vertical axis (z) according to the equation $(2Vo/\pi)\sin^{-1}(a/\sqrt{z^2 + a^2})$. The VE-field, however, decreases as a function of $\varphi = -(2Vo/\pi)(a/z^2 + a^2)$, which can be found easily by differentiating the voltage equation with respect to z, and the peak value of the VE-field at the surface (z=0, r=0) is $\varphi = -2Vo/(\pi a)$ or $\varphi = I/(2\pi\sigma a^2)$. We fit the VE-field equation to our data collected with the epidural placement of the electrode at its center while leaving Vo as a free parameter (Figure 2.2, center). The Vo value that fits the experimental data best for r=0 was also used to plot the VE-field equation at r=2mm and r=4mm from the edge of the stimulation electrode in Figure 2.2 (2mm and 4mm). The VE-field is shown as a 2D heat plot in Figure 2.3 for comparison with the experimental data and will be discussed at the end.

2.3 Results

2.3.1 VE-Fields with Epidural Injection of Current

The peak-to-peak voltage induced by the current pulse was measured as a function of depth down to 6mm from the dura surface (Figure 2.2, top row) at the center of the helix, and 2mm and 4mm away horizontally from the stimulation electrode (see Figure 2.1D).

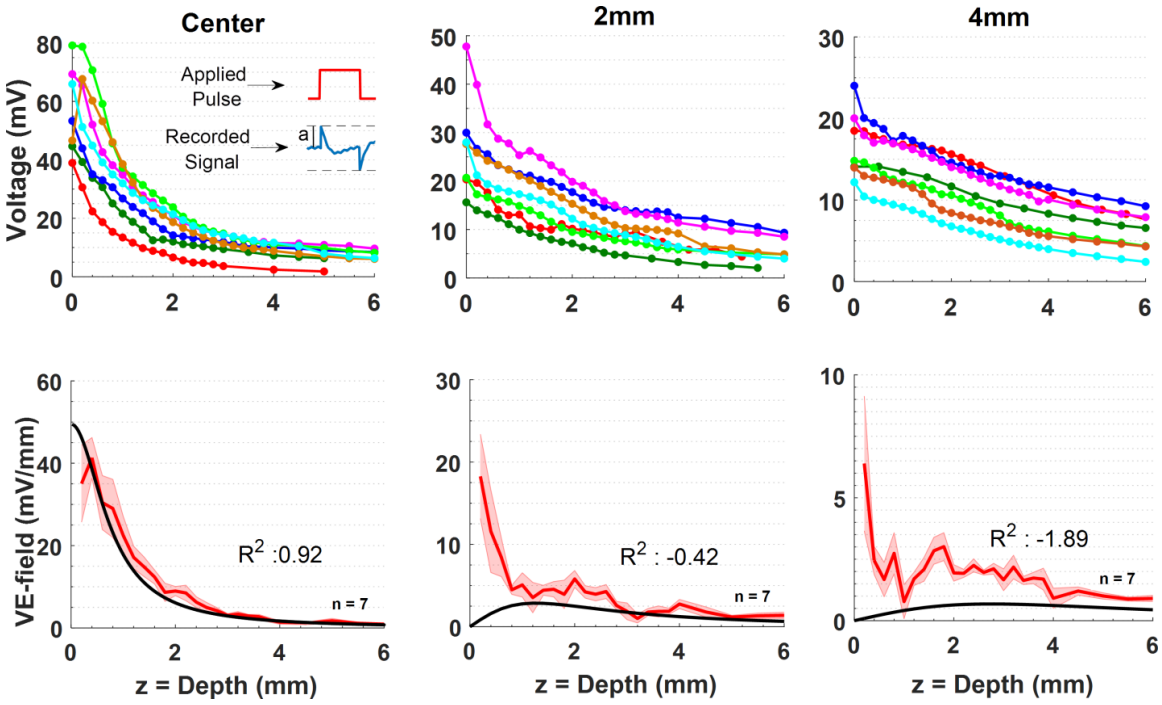

Figure 2.2 Voltage (top row) and VE-field (bottom row) measurements made with epidural (as in Figure 2.1D) placement of the Ag/AgCl helical wire stimulation electrode with 1.5 diam. Top Row Left to Right: Voltage measurements made with respect to a reference on the skull and via penetrations at the center, and 2mm and 4mm from the edge of the helical electrode. Seven sets of measurements were collected in five animals. In two sets, the voltage was measured at a fewer points below 3mm of depth. In such cases, exponential interpolation was utilized to estimate the missing voltage values. The inset depicts how the voltage amplitude (a) measurements were made at the rising edge of the recorded waveforms. Bottom Row: The mean of the vertical E-fields calculated by differentiating the voltage measurements shown in the top row for each penetration separately. The shaded areas indicate ± standard error. The black solid line is the VE-field predicted by the analytical equation derived by Wiley & Webster (Newman, 1966) that provided the best fit, i.e. highest coefficient of determination (R2), when Vo at V(r=0, z=0) is set to 58.3mV. For 2mm and 4mm penetrations, the analytical equation was evaluated (solid black lines) using the same Vo value for consistency.

Vertical electrical fields (VE-fields) were computed by differentiating the raw voltage measurements without any filtering or curve fitting, and averaged across the animals (Figure 2.2, bottom row). Note that the vertical offset in the voltage plots of the top row do not carry any significance since they can vary between animals depending on where the recording reference electrode is placed along the current pathways between the stimulation and the return electrodes. The voltage curves decline sharply under the stimulation electrode with maximum values underneath the dura (depth = 0mm), as expected. The VE-field was also maximum under the stimulation electrode (center, depth = 0mm) near the cortex, declined exponentially, and lost more than 75% of its strength by 2mm below the stimulation electrode and further decreased down to negligible levels by 6mm. The analytical equation by Wiley and Webster (see methods) was evaluated and fit to the VE-field by using Vo as the free parameter. The analytical formula provided a good-fit (R2 = 0.92) including the initial plateau near the cortical surface for Vo = 58.3mV. As the recording electrode was moved horizontally to 2mm and 4mm away from the stimulation site, the VE-field decline near the surface became sharper and an elevation appeared at deeper levels. The initial sharp decline was not predicted by the analytical equation since the semi-infinite model assumes a non-conductive medium above the surface and a zero vertical current at the boundary. The band of large VE-fields extending horizontally underneath the surface can also be appreciated from the heat plot of Figure 2.3A. Interestingly, for all penetrations (center, 2, 4mm) there seems to be a peak in the E-field near or a little above the 2mm mark, which may indicate a sharp change in tissue conductivity, e.g. from gray matter to white matter. The analytical equations fail to predict the VE-field amplitudes, in general, at 2mm and 4mm from the stimulation electrode with

the same Vo used at center penetration. Thus, the VE-fields expand more in the horizontal direction than predicted.

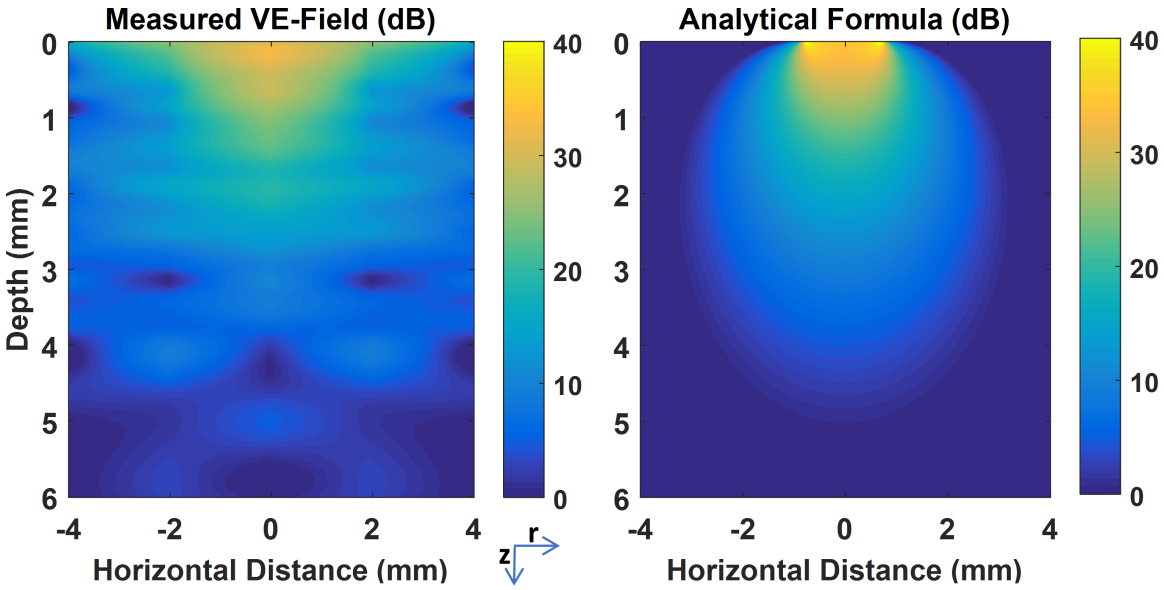

Figure 2.3 Vertical E-field distribution as a heat plot on a logarithmic scale. The left panel was obtained by linear interpolation of the measurements presented in Figure 2.2 and reflected over the vertical axis in the middle. The right panel is the predicted VE-field by the analytical equations of Wiley & Webster. Depth=0 corresponds to the surface of the cortex.

2.3.2 Comparison of VE-Fields with Current Injections over the Skin, Skull, and Dura

Figure 2.4 compares the VE-fields with three different placements of the helical electrode; over the skin, skull, and dura. The epidural stimulation produces the largest electric field intensities in the brain parenchyma while epidermal placement produces the lowest intensity, as expected, both at 2mm and 4mm horizontal locations from the electrode. Note that for over-the-skin and skull placements of the stimulation electrode the E-fields measurements were not in the center of the electrode in order not to disturb the intactness of the skin or skull with a penetration hole. The skin attenuated the VE-field (or shunted the electric currents) to a much larger degree than the skull, as seen with penetrations both

at 2mm and 4mm horizontal locations from the stimulation electrode. The over-the-skin placement did not produce an exponentially decreasing VE-field profile by depth as the other two placements of the stimulation electrode, and the VE-fields measured at the cortical surface (depth = 0) were about an order of magnitude smaller. The skin thickness was measured at the end of the experiment and found to be around 0.5mm under the stimulation electrode.

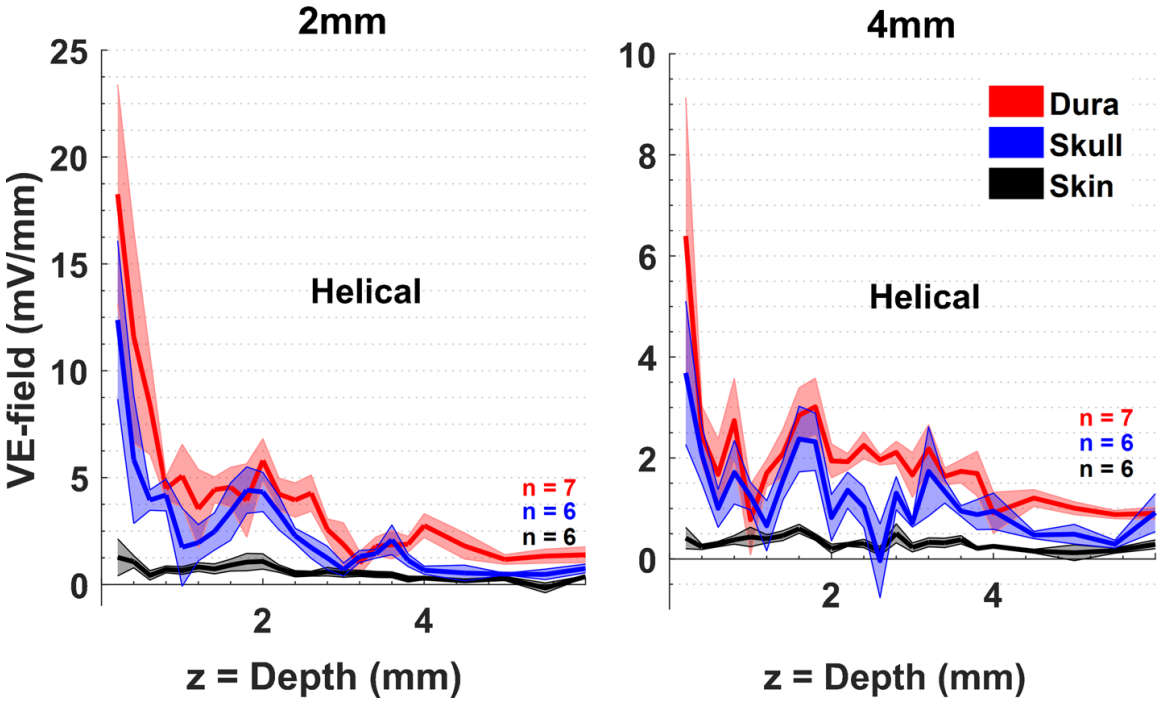

Figure 2.4 Comparison of VE-fields for three different placements of the helical wire electrode over the skin, skull, and dura mater. Measurements are repeated at 2mm (left) and 4mm (right) horizontal distances from the edge of the helical electrode. The averages of (n) measurement sets are plotted (solid lines) and the standard errors are shown as shaded areas.

2.3.3 Location of the Current Return Electrode

Lastly, we investigated how the location of the stimulation reference electrode affects the electric field strength in two rats. In the previous experiments, a Ag/AgCl wire inserted into the ipsilateral shoulder was used as the current return electrode (cathode). For this

experiment, three alternative sites were tested for the cathodic electrode: the contralateral shoulder, the submandibular muscles, and the ipsilateral hind limb. The epidural stimulation experiments with the helical wire electrodes were repeated against these reference electrode placements and the VE-fields as the difference of the voltage between the depths of 0.6–2.0mm were measured in nine different craniotomy holes (4 and 5 holes in two rats) as the stimulus was applied through the same hole. The maximum deviation from the ipsi-shoulder measurement was less than 1.36% with any of the new reference points. None of the VE-field measurement sets made at various depths from 0.6 to 2mm (N = 5) against the novel reference points were significantly different from that of the set against the ipsi-shoulder electrode (paired t-test, $p>0.5$).

2.4 Discussion

2.4.1 E-field Attenuation by Skin and Skull

The skin thickness changes around the head and rodents are no exception to this rule. Because of the compression we applied to hold the electrode down firmly on the skin, the skin thickness decreased under the stimulation electrode during the course of the experiment and found to be ~0.5mm at the end. The skin had to be removed also caudal to the stimulation electrode to make craniotomy holes at the recording points. Hence, we can only make general remarks about the skin effects on the E-field measurements in the face of these sources of variability and practical limitations. About a four-fold decrease occurred in the VE-field when the electrode was placed over the skin as opposed to the skull surface. The average skull thickness was measured to be ~0.5mm (N = 5). In agreement with this data, Vöröslakos *et al*. reported that transcutaneous stimulation generated several-fold

weaker electric fields compared to subcutaneous stimulation in rats (Vöröslakos et al., 2018). There was a relatively small loss of electric field intensity when the helical electrode was moved from the dural surface to the skull surface in our data.

With over-the-skin electrodes and 100μA current injection, the vertical electric field drops down to ~1mV/mm at 2mm and 4mm from the stimulation electrode (Figure 2.4). Terzulo and Bullock reported that the firing frequency of neurons can be modulated by voltage gradients as low as 1mV/mm (Terzuolo & Bullock, 1956), which is also the lower bound indicated by rodent studies (Ozen et al., 2010; Vöröslakos et al., 2018). The large variability in the skin thickness and its loose connection to the skull in the rat can make the results with epidermal montage highly unpredictable in behaving animals. Therefore, placing the electrode over the skull would be a reasonable compromise to avoid the variability introduced by the skin and to improve the focality of stimulation, while still avoiding large E-field peaks as they occur with epidural stimulation.

We did not measure the VE-field at the electrode center with over-the-skull electrodes. The epidural stimulations in Figure 2.2 show that the VE-field under the electrode decreases by about a factor of two from the electrode center to 2mm off the edge. If we can extrapolate from over-the-skull stimulations in Figure 2.4 at 2mm, the VE-field under the electrode should be about 25mV/mm at the cortical level. The current density at electrode-skull interface is 56.6 A/m2 for the helical electrode. For comparison, Bikson *et al*. (Marom Bikson et al., 2016a) computed the E-field at the cortical level for similar skull electrodes (2.1 mm) in the rat using finite element analysis (FEA) for the current density of 142.9 A/m2 (at the electrode surface) that was reported as the injury threshold by Liebetanz *et al*. (Liebetanz et al., 2009). If we upscale our predicted VE-field (25mV/mm)

at the cortical surface for their current density (142.9 A/m2), we find 63 mV/mm, which is about 50% higher than the cortical electric fields (42 mV/mm) computed in their FEA model. This discrepancy can be explained by the variations in the thicknesses and conductivities of the skull and CSF in experimental animals from the assumed values in their FEA model.

2.4.2 Non-homogeneity of the Brain

That the skull resistivity was much higher than that of the skin and brain tissue was first demonstrated by early intracerebral voltage measurement studies in human cadavers (Smitt & Wegener, 1944) and anesthetized monkeys (Hayes, 1950). Hayes predicted that the high conductivity of the skin and scalp would tend to make the electrical fields more uniform inside the brain. Our data with over-the-skin stimulation does not have the exponentially decaying profile by depth as in over the skull and dura stimulations, and thus agrees with Hayes' prediction in general. A particular aspect to note is the VE-field peak that occurred consistently at around 1.5-2mm depths in most plots where the gray matter transitions into the white matter and thus a significant change in local conductivity is expected. The lower conductivity of the white matter seems to cause an elevation in the VE-field at the border of the two regions. The fact that the VE-field decline in the gray matter is sharper at 2mm and 4mm horizontal locations than at the electrode center (Figure 2.2) must, however, be due to the higher conductivity of the cerebrospinal fluid near the surface, rather than the gray/white matter conductivity differences.

2.4.3 Monopolar vs. Bipolar Montages

Repositioning the return electrode from the shoulder to other muscles around the body introduced changes smaller than 1.36% in the VE-field. This confirms the results reported

from finite element models that the voltage profile near the anodic electrode is more or less the same with the monopolar montage so long as the large surface return electrode is placed far enough from the anode. The field steering effect begins to occur when the return electrode is brought near the stimulation electrode, hence approximating a bipolar montage (Bikson, Datta, Rahman, & Scaturro, 2010b; Noetscher, Yanamadala, Makarov, & Pascual-Leone, 2014). Moliadze *et al*. (Moliadze, Antal, & Paulus, 2010) reported that the stimulation effects can significantly change depending on the distance between the stimulation electrodes, even for the extracephalic placement of the return electrode (*e.g.*, ipsilateral upper arm vs. ipsilateral forearm) in the human. This result is surprising since the current flow patterns should not be affected by the position of the return electrode as long as it is on the same arm. The sensitivity of the results to the location of the return electrode may be higher with epidermal placement of the electrodes due to currents flowing through the highly conductive skin. A practical point raised by our data is that the Ag/AgCl wires deinsulated for several mm at the end and inserted into a muscle can conveniently serve as a return electrode, replacing the large surface transcutaneous electrodes used in other studies (Dockery, Liebetanz, Birbaumer, Malinowska, & Wesierska, 2011; Tanaka et al., 2013).

That the E-field declines sharply by distance with monopolar montages is advantageous for spatial selectivity if the targeted neural structures are near the brain surface but makes it difficult to achieve significant E-fields at deeper brain regions without causing extreme electric fields near the surface. Attempts to focus the electric field at subcortical brain regions using multiple electrodes will have to deal with this challenge. Horizontal E-field can be maximized using bipolar montages by placing both the cathode

and the anode around the head on the sides, if the targeted neural structures are inside the cortical sulci where the somato-dendritic axis of the neurons is oriented horizontally. A recent paper (Vöröslakos et al., 2018) proposed both spatial focusing and time-multiplexing of the stimulus currents via multiple dipoles in order to maximize the horizontal E-field at a focal point inside the brain by taking advantage of the slow time constant of the cellular membranes at subthreshold potentials. While the tES methods enjoy the benefits of being non-invasive, the challenge of focalization may remain as the main disadvantage of the technique in the long run.

2.4.4 Stimulation Waveform

In our protocol, substituting DC with pulsed stimulation allowed us to overcome the poor DC response of the tungsten recording electrodes. The brain tissue can be treated primarily as a resistive medium hence the recorded amplitudes to be independent of frequency, up to 10kHz and even higher ranges (Miranda et al., 2006; Ruffini et al., 2013) owing to the "quasi-static approximation". Thus, our amplifier's high cutoff (fc) was set to 10kHz, which has corresponding rise time of 15.9μs ($tr = 1/2\pi fc$) for a first-order filter. We took the amplitude measurements 1ms after the pulse transition, allowing several rise times for the signals to stabilize while still being much shorter than the time constant imposed by the lower cutoff frequency of the amplifier (tr = 15.9ms, 10Hz).

A sinusoidal waveform at a constant frequency (e.g. 1kHz) could also be used for the stimulus current in this study instead of rectangular pulses. A stimulus waveform with a single frequency would overcome the bandwidth limitations of the metal recording electrodes and the amplifier, which attenuates the harmonics of a rectangular waveform to different degrees and distorts the recorded waveforms. The advantage of the rectangular

waveform, however, is that any mechanical disturbance to the electrode tip during penetration manifests itself not only as a change in the measured amplitudes but also as a distortion in the waveform, and thus alerts the experimenter about the quality of the signals. With sinusoidal waveforms only the signal amplitude would change, which could escape the attention of the experimenter and lead to significant miscalculations of the E-field.

2.4.5 Comparison with Theoretical Models

Despite the fact that Wiley & Webster equation (Wiley & Webster, 1982) assumes a homogeneous medium, and does not account for the impedance of the electrode-electrolyte interface and the current redistribution across the electrode surface due to amplitude and frequency dependency of the interface (Cantrell, Inayat, Taflove, Ruoff, & Troy, 2007), it provides a reference point for comparison. The simplicity of using an analytical equation instead of building complicated models can be much more practical for quick estimations of the E-field underneath a monopolar electrode if that is all that is needed. Comparison of the experimental data with the theoretical model in 2D (Figure 2.3) reveals some fundamental similarities but also significant differences. Both plots show that the largest VE-fields occur under the electrode, but the experimental VE-field diminishes within the gray matter for the most part, subsiding to negligible levels in the white matter. In the experimental data the VE-field spreads more in the horizontal direction near the surface most likely due to the high conductivity of the CSF, and perhaps that of the gray matter also to a degree. The theoretical plot assumes a non-conductive medium above the brain and does not account for the presence of the skull. In addition, there are clearly regions of varying conductivities in the experimental data that cause inhomogeneities in the electric field. Lastly, the VE-peaks at the electrode edges that are suggested by the earlier analytical

models (Wiley & Webster, 1982) were not observed in the experimental data. This may be because of the distance (~0.5mm) allowed between the electrode surface and the brain cortex in our setup, or the spatial smoothing of the E-field peaks may be explained partially by the presence of the electrode-electrolyte interface as predicted by more advanced models (Cantrell et al., 2007).

2.4.6 Practical Considerations

The surface area of the electrode that is in contact with tissue primarily determines the E-field strength in the vicinity of the electrode. Therefore, epidural placement of the stimulation electrode may lead to large variations in the E-fields in the cortex if the electrode moves even by very small amounts. If the electrode contact area with the cortex is well defined, the simple analytical equations (Wiley & Webster, 1982) can become very useful for predicting the potential and the VE-field underneath the electrode. The equation for the VE-field at the surface ($z = 0$, $r = 0$) is $\varphi = -2Vo/(\pi a)$. For Vo value that gives the best fit with this equation to our data was found to be 58.3mV. Assuming a homogenous medium, an overall conductivity value of 0.57 S/m can be found by substituting this value of Vo into the Newman equation ($Vo = I/(4\sigma a)$), which is about three times higher than the commonly used conductivity for the brain (0.2 S/m) most likely due to the high conductivity of the CSF (1.65 S/m) (Datta, Elwassif, Battaglia, & Bikson, 2008). For a known electrode diameter and current, one can use this modified conductivity value to estimate the VE-field peak underneath the epidural electrodes. Having an accurate prediction for the vertical E-field near the surface, where most of the cortical neurons are found in an animal with a lissencephalic brain like the rat, can prove to be useful when direct measurements of the field is not possible.

The current distribution across the disk electrodes is predicted to suffer from edge-effects by earlier models (Wiley & Webster, 1982). Inclusion of the electrode-electrolyte interface into the model produces a more uniform current profile across the surface, although the effect is amplitude and frequency dependent (Cantrell et al., 2007). The choice of the electrode material thus is crucial to minimize the electrode-electrolyte impedance and improve reproducibility. In order to prevent the edge-effects from influencing the E-field distribution inside the brain, the stimulation electrode can be kept at a distance from the superficial layers of the cortex. The skull can serve as a spacer in this case. The disk electrode can be attached onto the skull at reproducible stereotaxic coordinates and the top of the electrode can be covered with some nonconductive material to prevent current spreading through the skin. The skull thickness at the point of electrode placement can be standardized to a degree by controlling the weight/age of the animal. Alternatively, one can also make a craniotomy hole and fill it with conductive gel or isotonic saline and position the stimulation electrode at a known distance above the cortex as we did with epidural stimulations. Because normal saline has a conductivity (1.65 S/m) that is about eight times higher than that of the brain (0.2 S/m), the stimulation electrode may electrically be assumed to be at the cortex/saline interface for practical purposes. The highly conductive saline may however be replaced with encapsulation tissue by time in chronic implants. For most reproducible results, the E-field should be measured directly inside the tissue in each animal separately if this can be done without disturbing the intactness of the neurons or the E-field itself.

2.5 Conclusions

This paper provides experimental data as a reference study for more realistic estimates of the electric fields induced in the rat brain during tES studies. The skin attenuates the electric field much more strongly than the skull and causes the current spread more uniformly inside the skull. For focal stimulation, it may be best to place the stimulation electrode on the skull to avoid the skin effect. The electrical field perpendicular to the cortex decreases exponentially near the surface and loses most of its strength within 2mm into the brain underneath the electrode and within 1mm of depth off of the electrode edge. A 100μA current injected through a 1.5mm over-the-skull electrode is predicted to generate ~25mV/mm at the cortical surface. For epidural placements of the stimulation electrode through a craniotomy hole, a modified value of 0.57 S/m for the brain conductivity can be assumed to estimate the voltage at the cortical surface using the volume conductor equations. Significant E-field peaks occur in the brain parenchyma, most likely due to local conductivity changes, especially at the gray/white matter border. These large fluctuations in the E-field measurements show that the homogeneous volume conductor assumption is too simplistic for modeling the local effects of the injected current.

CHAPTER 3

MODULATION OF THE CEREBELLAR PURKINJE CELL ACTIVITY WITH ELECTRICAL STIMULATION

3.1 Objective / Background Information

Electrical neuromodulation methods provide therapeutic interventions for a wide variety of neurological disorders. Low intensity transcranial electrical stimulation (tES), in particular, has drawn significant attention for its clinical potential because of its non-invasiveness, minimal or no side effects, and the simplicity of the required equipment (Antal, Alekseichuk, Bikson, Brockmoller, et al., 2017; M. Bikson et al., 2016). Thus, optimizing the efficacy of this clinical tool becomes significant and doing this requires understanding how tES alters neuronal function at the cellular level. In general, animal studies have shown that currents applied across brain regions shift the resting membrane potential of neurons, and thus it is currently hypothesized that the mechanism of action underlying tES is the altered neuronal excitability resulting from these shifts in the membrane potential (L. J. Bindman et al., 1964; Pelletier & Cicchetti, 2014). Depending upon the applied electric field direction relative to the neuronal axis, this alteration can be either excitatory or inhibitory (Bikson et al., 2004a; Radman et al., 2009b). In addition to the acute cellular response (Liu et al., 2018; Radman et al., 2009b), synaptic plasticity effects are also likely and may contribute to the therapeutic action of tES (Bikson, Paulus, Esmaeilpour, Kronberg, & Nitsche, 2019).

The cerebellum has been a target of electrical neuromodulation in part because of its central role in motor control. The growing body of evidence showing cerebellar involvement in cognitive functions (Buckner, 2013; Van Overwalle, Baetens, Mariën, &

Vandekerckhove, 2014) will likely make the cerebellum an even more frequent target. Thus, understanding how tES acts on the cerebellum, and of how this action alters the activity of brain regions that receive cerebellar output, becomes significant. Regarding the first issue, the cerebellar cortex, as opposed to the deep cerebellar nuclei (DCN), is likely to be the main area that is directly affected by tES, given its superficial location. Although tES will likely affect multiple classes of cerebellar cortical cells, the Purkinje cell (PC) is the sole output neuron, making characterization of its responses a key issue. Purkinje cells generate simple and complex spikes, the former spontaneously and in response to granule cell inputs, and the latter driven by climbing fiber activity. The spatiotemporal pattern of simple and complex spikes is important because synchronous PC activity sculpts the output of the DCN (Blenkinsop & Lang, 2011; De Schutter & Steuber, 2009; A. L. Person & Raman, 2011; Tang, Blenkinsop, & Lang, 2019). The DCN, in turn are the major output station of the cerebellum, projecting, via the thalamus, to widespread regions of the cerebral cortex, including motor, prefrontal, and parietal cortical regions. Thus, altering PC activity with tES provides a way to modulate cerebellar outputs that influence a large number of sites in the cerebral cortex that underlie diverse functions.

Transcranial direct and alternating current stimulations (tDCS/tACS) are two promising forms of tES and the cerebellum has been the target for both. Indeed, clinical studies have shown that cerebellar tDCS and tACS can enhance motor and cognitive functions (Block & Celnik, 2013; Hardwick & Celnik, 2014; P. A. Pope & Miall, 2012). For example, Galea *et al*. tested the effect of anodic and cathodic tDCS on cerebello-brain-inhibition (CBI) and showed that CBI was augmented during anodal tDCS and reduced during cathodal tDCS, demonstrating that the effect of tDCS can be polarity dependent

(Galea, Jayaram, Ajagbe, & Celnik, 2009). An analogous polarity dependency for AC currents was shown by Chan *et al*. who applied alternating currents in an *in vitro* turtle cerebellum preparation. They reported that during the positive phase the current hyperpolarized the apical dendrites and depolarized the soma, leading to increased spiking, and that the opposite effects occurred during the negative phase (Chan, Hounsgaard, & Midtgaard, 1989; Chan et al., 1988; Chan & Nicholson, 1986). For tACS this polarity dependence raises the possibility that the local field potential oscillations that occur in the cerebellum could be entrained with tACS, as has been demonstrated for slow oscillations in other parts of the brain (Helfrich et al., 2014; Ozen et al., 2010; Zaehle et al., 2010).

In vivo animal studies addressing questions related to the mechanism of cerebellar tDCS and tACS are scarce in the literature (Krause, Vieira, Csorba, Pilly, & Pack, 2019), which is problematic as significant differences exist between *in vivo* and *in vitro* conditions. Thus, our goal was to investigate the response of the cerebellar cortex to these neuromodulation paradigms at the cellular level. Our results demonstrate that PC simple spike activity is modulated and strongly entrained by AC stimulation over a large range of frequencies. Moreover, PC responses showed a dependence on direction of the electric field, with significantly stronger modulation caused by rostrocaudally oriented fields as compared to fields applied mediolaterally. For tDCS, we also observed a sharp transient response at the onset and offset of the stimulation current. The results of this study shed light on some basic mechanisms of cerebellar neuromodulation by tES that can help design future human trials.

3.2 Methods

3.2.1 Animal Surgery

Ten Sprague Dawley rats (300-350g, male, Charles River) were used in this study to obtain PC recordings. All procedures were approved and performed in accordance to the guidelines of the Institutional Animal Care and Use Committee, Rutgers University, Newark, NJ. Animals were first anesthetized with 5% isoflurane in an induction chamber and maintained between 1-2% during the course of surgery. Then, they were moved to a stereotaxic head frame, and body temperature was measured with a rectal probe and regulated with a heating pad under the animal (ATC 1000, WPI). Blood oxygen level was monitored with a pulse oximeter attached to the hind paw and made sure to stay above 92% during recordings. The hair over the head was shaved and a midline skin incision was made to expose the skull over the cerebellum. The entire back side of the cerebellum was opened with rongeurs. The dura mater was left intact and kept under warm saline (measured as ~34°C using infrared thermometer) to prevent dehydration and cooling of the cerebellar cortex. The stereotaxic frame was placed inside a Faraday cage to eliminate electromagnetic interference in neural recordings. About 10 minutes before starting to record neural activity, the animal was transitioned from gas anesthesia to ketamine/xylazine mixture (80mg/kg and 8mg/kg, IP), since most other studies on cerebellar electrophysiology were conducted under this anesthesia regime, and additional doses of ketamine (20mg/kg, IP) were injected as needed.

3.2.2 Electrical Stimulation

To generate E-fields directed along specific axes, a stimulation electrode platform was built using four 125µm thick Ag/AgCl wires that were affixed on a 4x4x1mm silicon

(Polydimethylsiloxane; PDMS) board in a rectangular configuration (Figure 3.1A). The distance between opposite contact pairs was 3.5mm and the length of each contact was slightly shorter (~3.2mm). Another Ag/AgCl wire was wrapped 3 times around a 1mm diameter drill bit to make a helical electrode. After opening a 1.2mm circular hole at the center of the substrate, the helical electrode was positioned into this hole. Opposing wire electrode pairs (shown in blue and red) were used to generate E-fields in the mediolateral or rostrocaudal directions. The helical electrode was used to create E-fields in the dorsoventral direction by pairing it with a Ag/AgCl wire inserted into the right hind limb. The electrode pairs were connected to the output of a voltage/current isolator unit (Model 2200, A-M Systems) through a commutator that facilitated switching between the electrode sets quickly. The PDMS substrate was placed over the cerebellum with its center positioned over vermis lobule 7 and secured with silk sutures tied to the frame. The hole in the center was filled with normal saline to ensure a stable interface with the helical electrode.

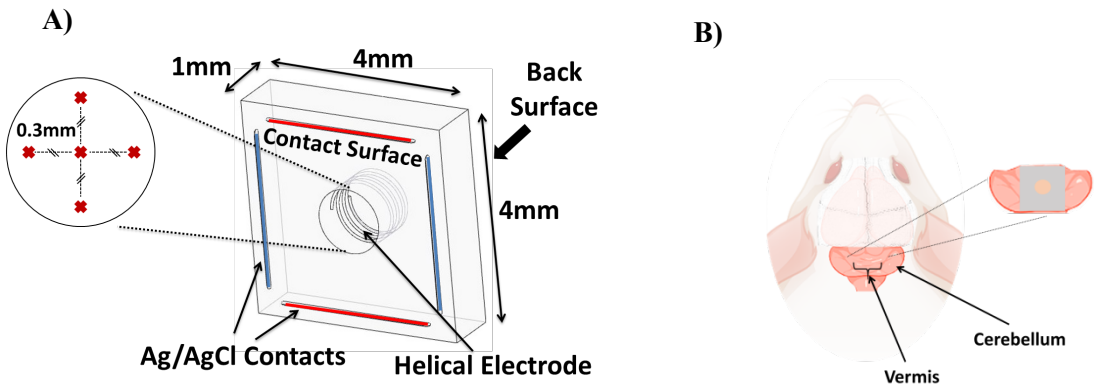

Figure 3.1 A) Computer drawing of stimulation electrode. Four Ag/AgCl wires were affixed on the PDMS substrate as shown and used to apply e-field from ML (red pair) and RC (blue pair) directions. Another Ag/AgCl helical electrode was placed in the central hole to apply stimulation in the dorsoventral direction. The circle on the left end represents the hole opened at the center of PDMS stimulating electrode and red X's show points for E-field measurements. B) Schematic showing the placement of the stimulation electrode on the cerebellar cortex with its center on lobule VII of the vermis.

3.2.2.1 AC Stimulation. Once stable spike activity was detected from a cell that was identified as a PC from its characteristic complex spikes, ten-second long sinusoidal currents were applied to the cerebellar cortex in the dorsoventral, mediolateral, and rostrocaudal directions by switching to respective electrode pairs sequentially. Sinusoidal stimulus frequency was varied systematically from 2Hz to 100Hz and the amplitude was varied from 50μA to 600μA in steps.

3.2.2.2 DC Stimulation. A direct current (DC) was applied to the cerebellum through the rostrocaudal electrode pair only for 20s. One or two intensity levels between 200-300μA were tested. The current was injected in both directions through the electrode pair with a settling period between applications that allowed the activity to return to its baseline level.

3.2.3 E-field Measurements

Two additional male SD rats similar in size to those used in stimulation experiments were anesthetized to measure the E-fields generated in the cerebellar cortex corresponding to specific current amplitudes. Five-second long sinusoidal currents, with 100 μA peak amplitude and 100 Hz frequency, were applied to the cerebellar cortex through the dorsoventral (DV), mediolateral (ML), and rostrocaudal (RC) electrode pairs as in the stimulation sessions. A glass micro-pipette mounted on a micromanipulator was inserted into the cerebellar cortex at five selected positions within the central hole of the stimulation electrode (Figure 3.1A, inset). Voltage measurements were obtained at depths of 200, 250, and 300 μm from the pial surface. At every recording position and depth, sinusoidal current was applied via each one of the three sets of electrode pairs. The ML and RC E-field components were calculated by taking the difference of the voltages measured at a depth

of 250 μm by an appropriate pair of recordings (two of the four peripheral recording positions) and dividing by separation (0.6 mm). The central recording position was used to measure the E-field component in the DV direction by taking the difference of the voltages at 200 μm and 300 μm depths and dividing by the difference in depth (100 μm). For each electrode pair, the E-fields in three orthogonal directions were calculated. The results in all PC modulation trials were expressed as a function of E-field strengths by converting the applied current amplitudes to E-fields based on these measurements. Note that the E-fields measured only at 250 μm because that depth approximately corresponds to the PC layer. The E-field is not expected to be uniform in any direction in this setup. Thus, the E-field measurements are made to provide a reference point only when comparing with other studies.

3.2.4 Data Collection and Analysis

To record PC activity, a glass micropipette (3-5MΩ) filled with normal saline was inserted at the center of the hole of the electrode platform using a 3-axis 10μm-resolution micromanipulator through the dura and pia maters into the apex of lobule 7. Recordings were filtered at 100Hz-10k and amplified (Model 2200, A-M Systems, Carlsborg, WA) with a gain of 1,000 or 10,000, depending on the spike amplitude, and sampled at 100kHz onto the computer via data acquisition board (NI, PCI-6071). A total of 23 PCs were recorded in 10 animals, with a maximum of three PCs in a given animal. Neural signals were monitored simultaneously on an oscilloscope and audio speaker.

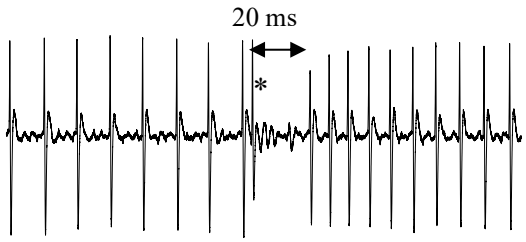

Figure 3.2 An example of a Purkinje cell recording demonstrating a short pause in the simple spikes following a complex spike (star).

PCs were identified by their characteristic complex spikes, which were typically followed by a 10-30ms pause in SS activity (Figure 3.2). Recordings were all obtained at depths of ≤250μm to ensure that they were located at the apex of the lobule and thus we would know the orientation of their dendritic tree with respect to the stimulation electrodes. For each stimulus setting, baseline PC activity was recorded before and after the stimulus period. For AC stimuli the pre- and post-stimulation periods were each 5s, with an intervening 10-s stimulus. For the DC stimuli pre- and post-stimulation periods were 5s and 10s, respectively, and the stimulus was 20s in duration.

Spikes were detected offline in Matlab (Mathworks) with a threshold-based spike detection algorithm. For high frequency AC stimulation, recorded signals were pre-filtered with a sharp high-pass at 200Hz, in addition to the 2nd order filters in the amplifier, to suppress the stimulation artifacts.

3.3 Results

3.3.1 E-Field Measurements

The cerebellar cortex is highly anisotropic, with many neuronal elements oriented along specific and often perpendicular axes. Because of this, the direction of the E-field may be

a particularly important parameter for cerebellar stimulation, as different classes of neuronal elements may be activated by fields in different directions. Before examining this issue in detail, we first tested the ability of the stimulus electrodes to generate E-fields directed along the RC, ML and DV axes. The results show that each stimulus electrode pair produced an E-field whose amplitude was largest in the intended direction (*i.e.*, along the axis connecting the two electrodes) but that smaller amplitude fields were present in the other two orthogonal directions. A 100μA current applied between the specific RC, ML, and DV electrode pairs produced 1.5, 1.5, and 7.5 mV/mm fields in the direction of the electrode pair. For each electrode pair, the fields produced in the other two orthogonal directions were <30% of these maximal fields, confirming that the stimulation electrode produces a directional E-field.

3.3.2 Spontaneous Simple Spike Rates

To have a baseline for comparing the evoked activity, spontaneous PC simple spike activity was characterized. PCs had a mean firing rate of 40±20 Hz (mean±std) (n=23) before any stimulation applied. We also compared the firing rates before and after stimulation for each intensity level separately. The paired t-test failed to show any significant effect at any current level ($p<0.11$) as compared to the baseline individually. Thus, stimulation did not cause any immediately occurring lasting changes in firing rates. However, spontaneous variations in simple spike instantaneous firing rates and at longer times scales were present in all PCs (Figure 3.3, pre- and post-stim periods). Modulation index values of the spontaneous variations were calculated for each cell using the pre-stimulation periods 0.82±0.45 (mean±std). These spontaneous variations could be obscured by stimulus-evoked activity but reemerged after the stimulus was terminated.

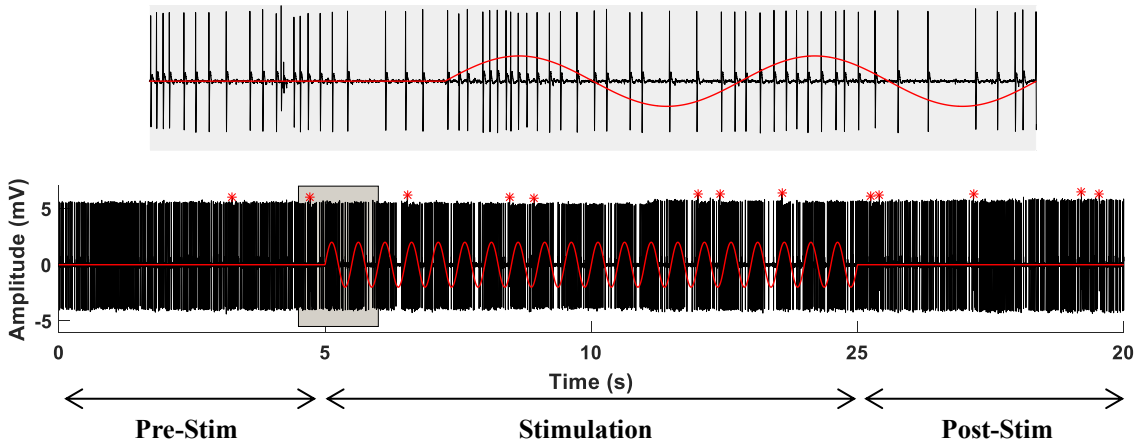

Figure 3.3 An episode of Purkinje cell activity during rostrocaudal AC stimulation with 3mv/mm amplitude. The red sinusoidal trace represents the injected current at 2Hz. The upper row shows a short segment of the recorded signal on an expanded time scale where the spike frequency increases during positive cycles of the stimulus current and vice versa. Complex spikes are marked with red asterisks.

In order to determine if the spontaneous activity changes over the course of the experiment, spontaneous MI values during the 5 s periods before the onset of stimulations in each E-field direction were calculated. These spontaneous MIs did not differ significantly, indicating that the spontaneous variations in the firing rate did not differentially influence the calculation of the MI values in different directions. This result also shows the absence of the after-effects of the simulation on the spontaneous modulation, in addition to the firing rate.

3.3.3 AC Stimulation

3.3.3.1 SS modulation varies with E-field direction and intensity. Figure 3.4A shows how the response of a typical cell to a 2Hz AC stimulation varied with stimulus amplitude for a field directed in the RC direction. In this case, the firing rate increased during the positive phase and decreased during the negative phase and was completely

suppressed at the higher intensities. The maximum SS firing rates occurred slightly before the positive peak of each cycle. In general, the exact phase relationship between the stimulus current and PC firing rate changes varied between cells. In fact, increasing or decreasing spiking could be associated with either the anodic or the cathodic phases of the stimulus, and peak firing rates did not necessarily coincide with stimulus peaks. To quantify this modulation, a modulation index (MI) was defined as the standard deviation of the inter-spike intervals (ISI) divided by the mean ISI for the period in question (in this case the duration of the stimulus). For the cell in Figure 3.4, the modulation index was highly correlated with stimulus intensity (Fig. 3.4B; $r=0.99$, $p = 0.0012$, test of whether $r \neq 0$).

The MIs were similarly calculated and plotted as a function of intensity for all 17 PCs (out of 23) that were tested in all three directions (Figure 3.5A), and the slopes of the regression lines fitted to individual cells were also compared (Figure 3.5B). From these plots, it is clear that RC- and DV-directed currents were the most consistent in producing a positive relationship between modulation depth and E-field strength, with 17 for RC and 15 for DV cells showing positively sloped regression lines. ML-directed currents produced generally weaker relationships, with about half of the cells showing negatively sloped regression lines. MI slopes in DV direction were significantly higher compared to ML direction (Figure 3.5B). Nonetheless, the MI slopes could be contaminated by spontaneous variations, particularly at low AC intensities and in the ML direction where the modulation is the weakest. The MI values, rather than slopes, measured at a single E-field (7.5mV/mm) were compared between all directions (Figure 3.6). RC modulation was again significantly stronger than the other two directions (RC>ML, $p=0.013$; RC>DV, two-sided, paired t-

test, p=0.027), however, DV was not significantly different than ML (two-sided, p=0.24). In order to check if ML stimulation caused modulation above the noise level, we compared the MIs at this E-field intensity with the pre-stimulus period and found no significant difference (p>0.056).

Spontaneous changes in firing rate are a source of noise that lowers the correlation (R^2) of the fitted lines. However, electrical stimulation for both DV and RC directions decreases the spontaneous variations and forces PCs to fire more regularly, as suggested by higher correlation of the line fit. The RC and DV directions generate higher R^2 values (0.69±0.32 (mean±std) and 0.74±0.31 respectively) compared to ML (0.43±0.34), which agrees with the example in Figure 3.4 showing significant entrainment of the SS activity during RC stimulation.

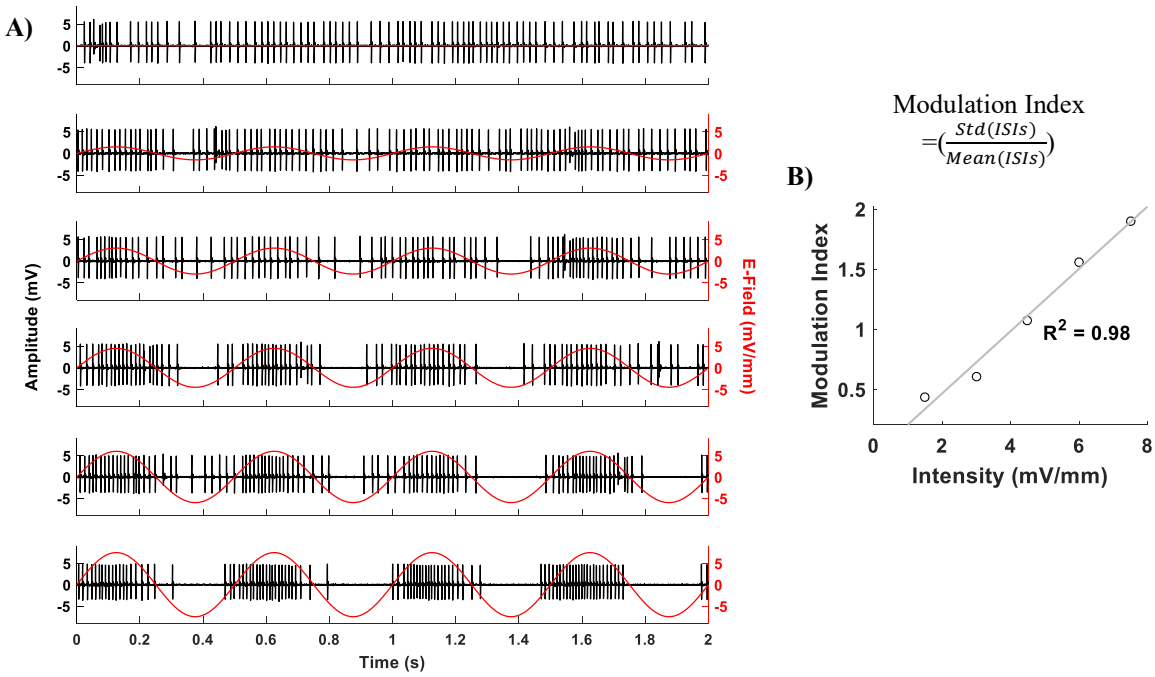

Figure 3.4 A) A typical PC response at varying amplitudes of 2Hz sinusoidal E-field applied rostrocaudally in an ascending order, indicated by the red traces. The first row contains the baseline PC activity. The spike frequency increases during positive phases and decreases during negative phases of the stimulus current, although some phase shift may also be present. The level of spike-frequency modulation is correlated positively with the applied E-field intensity in this example. **B)** Modulation index vs. stimulation current intensity for the recordings shown on the left.

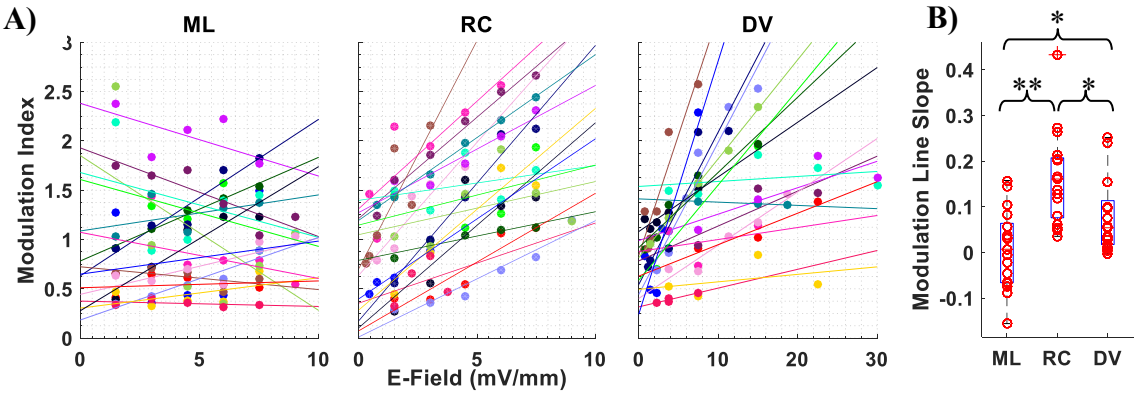

Figure 3.5 A) Incremental levels of E-fields are applied to the cerebellar cortex in mediolateral (ML), rostrocaudal (RC) and dorsoventral (DV) directions respectively and modulation indices are plotted from a total of 17 PCs, coded by the same color in all three plots. Each dot represents a single episode of recording at a specific E-field strength from the PC. Linear lines were fitted to the modulation index values at different E-fields separately. **B)** Box whisker plots for comparison of modulation effectiveness for E-fields in different directions. Each circle represents a slope of a specific line in figure 5a. Two-sided paired t-tests indicate that RC stimulation generates significantly higher modulation level compared to both ML (**p<3x10-6) and DV (*p<3x10-3) directions. DV also generates significantly higher modulation than ML direction (*p<0.015). (+): outliers.

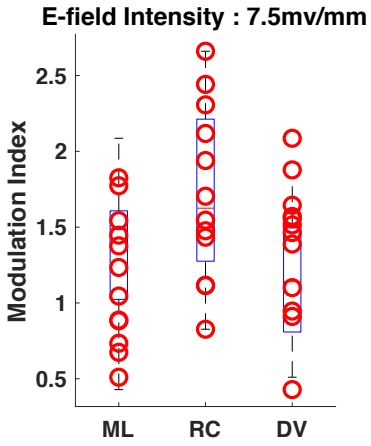

Figure 3.6 Direct comparison of modulation indices between different E-field directions at a single intensity of 7.5 mV/mm.

3.3.3.2 Entrainment to AC Cycle.

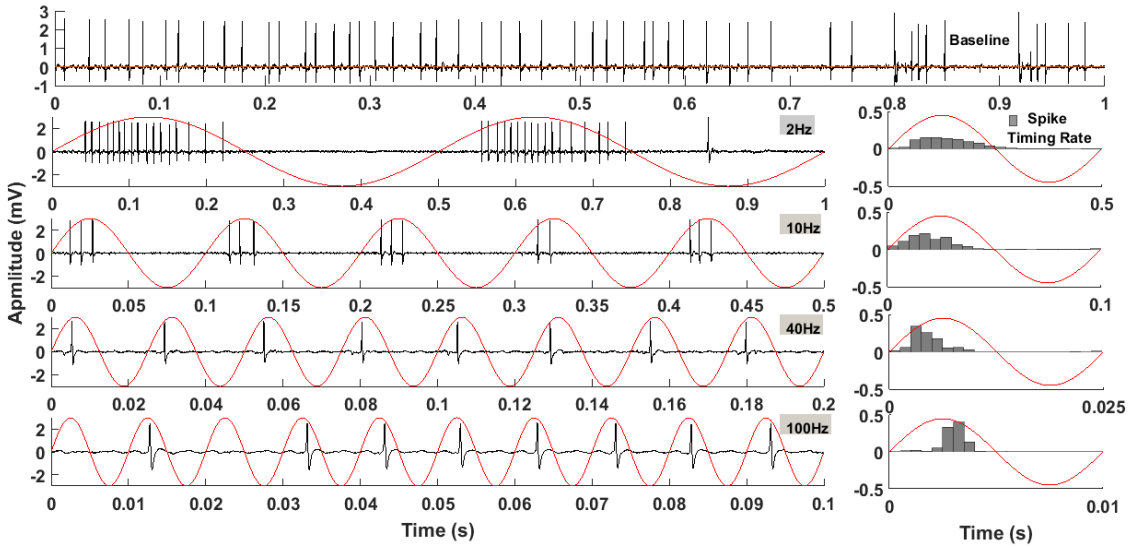

Figure 3.7 PC response to varying AC frequencies applied rostrocaudally with 4.5 mv/mm intensity. The first row shows the baseline PC activity, and rows below demonstrate the PC response to AC stimulation at 2, 10, 40 and 100 Hz respectively. The PC activity synchronizes with applied AC cycles. The activity pattern within each cycle is burst-like at low frequencies of the stimulus, whereas at higher frequencies the number of spikes that occur in an AC cycle decreases and spike timings become strongly locked to the stimulation cycle. Histogram plots on the right show the number of spikes that occur at specific time points during the stimulation cycle. The cycle was divided into 20 time bins.

Figure 3.7 summarizes the behavior of a PC under varying AC frequencies. The simple spikes fire with ISIs changing in a wide range when there is no stimulation, and once the stimulation is initiated, the spike timings begin to synchronize with the AC stimulus phase. At low frequencies, multiple spikes occur during the positive phase and the PC completely ceases firing in the negative cycle in this example. As the stimulus frequency is increased, the number of spikes that occurs during each positive phase decreases and begin appearing at much more specific time points with respect to the stimulation cycle (phase locking). When the AC frequency is raised up to 40Hz, which is around the mean spontaneous firing rate of this PC, only one spike fires per cycle and their timings are perfectly phase-locked

to the stimulus. Further escalating the frequency to 100Hz results in an increase in the overall firing frequency of the PC with one spike occurring almost during each AC cycle but missing some cycles. The bar plots on the right show the timing of the PC spikes with respect to the AC cycle. Phase locking becomes stronger with increasing frequencies as clearly seen in these bar plots.

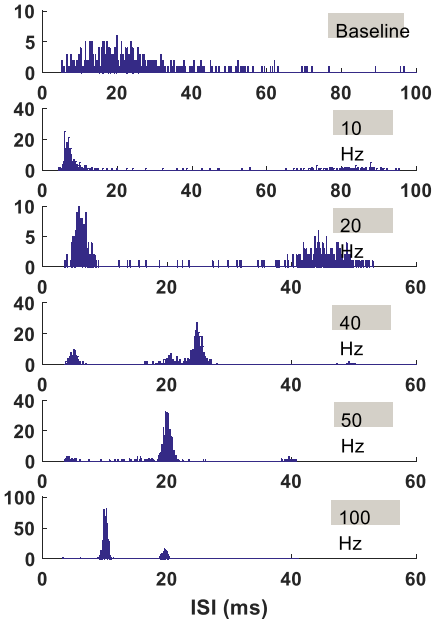

Figure 3.8 Inter-Spike-Interval (ISI) distribution at different stimulation frequencies. ISIs scatter in a large range during the baseline activity. Low frequency AC applications at 10 and 20 Hz cause a peak at short ISIs around 6 ms. With the increase of AC frequencies, ISIs gather around the values that corresponded to the stimulus cycle lengths, and their multiples.

During the baseline activity, the PC spike trains were characterized by positively skewed ISI distributions with a peak of 28ms ± 33ms (mean±std) (n = 174) on average (Figure 3.8 top panel). AC stimulation produced dramatic frequency-dependent changes in the ISI distribution. Stimulus frequencies lower than the spontaneous firing rate made a peak appear at the lower end of the ISI plot around 5ms (Figure 3.8, 10 Hz), reflecting the

high frequency bursts that occurred within each cycle. A smaller secondary peak occurred at ISIs roughly corresponding to the interburst period at the same time (80-90ms). As the stimulus frequency is further increased, additional peaks reflecting the subharmonics of the stimulus frequency appear when some of the AC cycles are skipped by the spikes (e.g. at 50ms for 40Hz). For progressively higher frequencies, the peak for bursting ISIs reduces and the main peak corresponding to the stimulus period increases in size (for 20-100 Hz panels), and because the burst length decreases with frequency, the main peak increasingly becomes narrower around the stimulus period. This effect of burst length is most evident for 40Hz stimulation in the skewed values of ISIs below 25ms extending down to 18ms, which is because the ISI between the last spike in a cycle and the first spike in the next cycle are less than the length of one cycle.

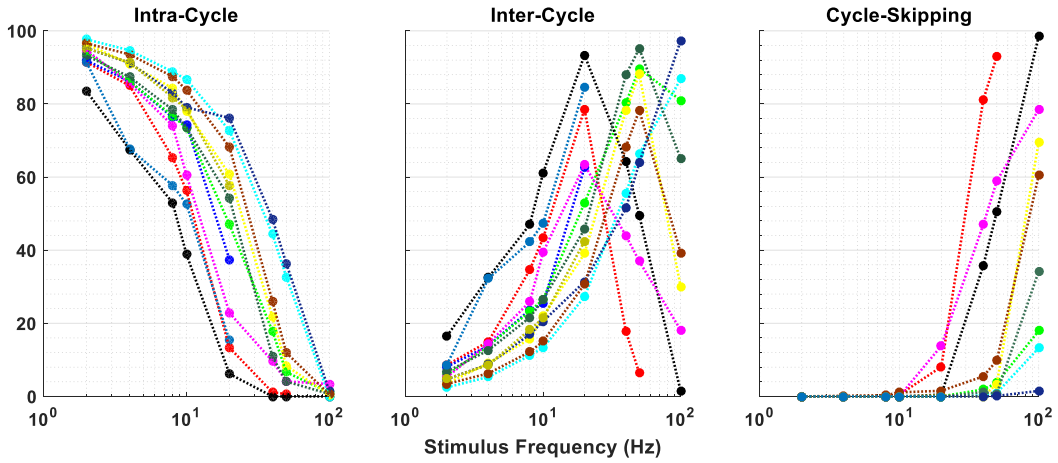

Figure 3.9 Percent of different ISI types as a function of stimulus frequency. ISIs were divided into three groups: intra-cycle, inter-cycle, and cycle-skipping. Each color represents measurements from a specific PC. Twelve different PCs were used in this analysis, and color coded. The percentage of intra-cycle spikes is high at low frequencies and decays when the AC frequency is increased, as also seen in Figure 3.7. In each cell, the AC stimulus intensity was selected such that the modulation depth was clearly appreciable through the audio monitor and retrospectively found to be within 1.5-6 mV/mm range.

Interspike intervals were calculated and then grouped into three categories: *intra-cycle*, *inter-cycle*, and *cycle-skipping* ISIs (Figure 3.9). The *intra-cycle* group contains ISI values where successive spikes occur within the same cycle. The ISI between the last spike in a cycle and the first spike in the next was labeled as an *inter-cycle* ISI. Finally, when the distance between spikes was more than one cycle of AC stimulation, indicating a cycle was skipped, these ISIs were classified as *cycle-skipping* group. For each PC, the number of ISIs for each category was then divided by the total number of ISIs in all groups for normalization, i.e. the sum of percentages across the three plots for the same PC at a specific frequency is equal to 100% in Figure 3.9. At low frequencies, a large percentage of spikes were labeled as *intra-cycle*. As the frequency increased, the percentage of *intra-cycle* spikes decreased and the other two groups increased. That is, the spikes per cycle became fewer in number and thereby the other two groups increased as percentages. With further increases in the stimulus frequency, at some point between 20Hz-50Hz, there is only one spike per stimulus cycle, at which point all ISIs are classified as *inter-cycle* type. In a cell where the entrainment is perfect, i.e. there is only one spike per AC cycle and no cycles are skipped, the *intra-cycle* and *cycle-skipping* groups would be zero percent, and the *inter-cycle* group would be 100%. Most of the cells were able to track the stimulation frequency up to ~40Hz, i.e. 0% of *cycle-skipping*. When stimulus frequency was increased above 50Hz these cells started missing cycles. At 100 Hz, only three cells could produce spikes in at least 80% of the AC cycles, as seen in the middle panel.

Finally, we questioned if the maximum entrainment frequency of a cell was determined by its spontaneous firing rate. However, the spontaneous firing rate of the cells

was not correlated to the highest frequency up to which the cells could be entrained by AC stimulation (R=0.003).

3.3.4 DC Stimulation

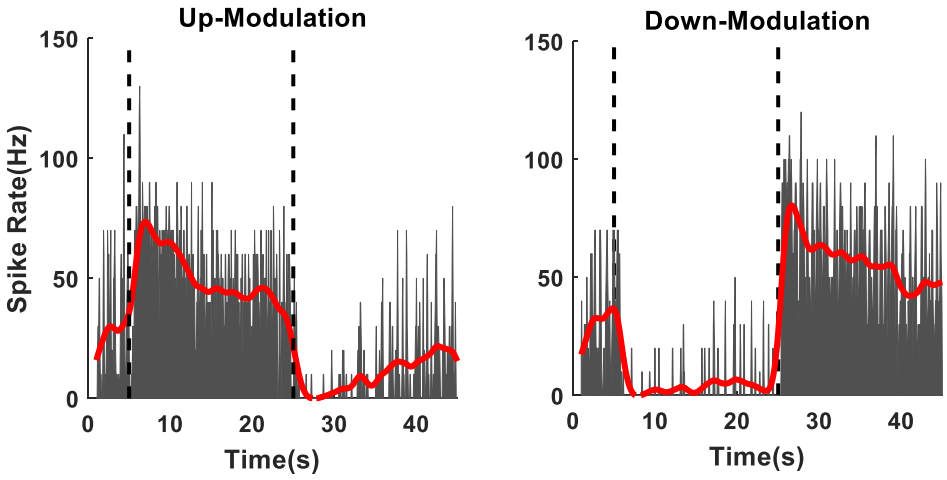

Figure 3.10 Firing pattern of a PC during DC modulation. The mean firing rate as a function of time was calculated in a 100ms sliding window and fitted by a smoothing spline (red trace). Sharp shifts in the spike rates were observed at the onset and the offset of the DC stimulation, and the observed effect was reversed based on the polarity of the stimulus.

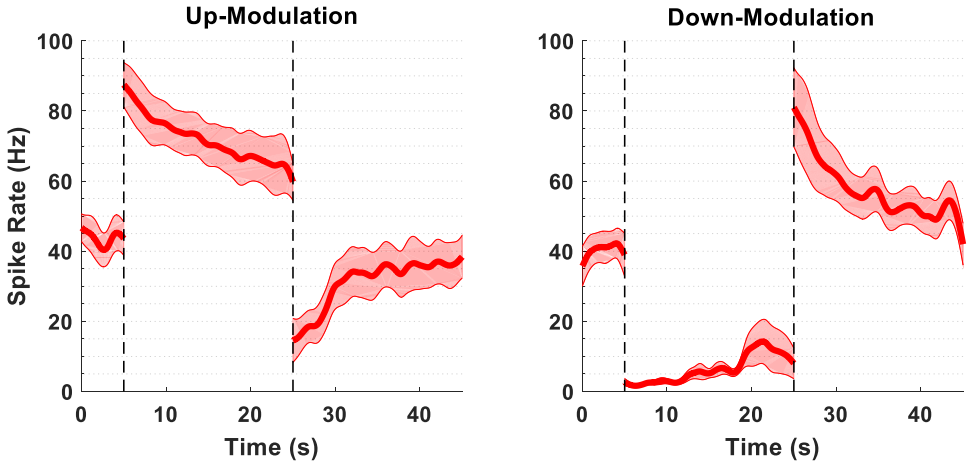

Figure 3.11 The mean spike rates from 6 different PCs during DC stimulation as a function of time. The shaded areas represent the standard error (SE). Dotted lines show the onset and offset time points of the stimulation.

DC current injections were made using the RC electrode pair because of the stronger modulation observed in this direction with AC stimulation. Recordings were divided into three time intervals: pre-, post-, and during-stimulation periods. For each time interval, the mean firing rate was calculated within a 100ms sliding window with 50ms overlap. Anodic and cathodic stimulation (named with respect to the rostral contact) modulated the spike rates in opposite directions in each cell (Figure 3.10), but not always in the same directions in different cells. As clearly seen in the average activity from multiple cells in Figure 3.11, the up-modulation response of the cells during stimulation consisted of two phases (Figure 3.11 left): an initial large transient response at the onset of the stimulus followed by a settling phase. However, the time constant for the firing frequency to return to a stable level could not be captured within the 20s window of recording. At the onset of down-modulating pulses (Figure 3.11 right), there is a dramatic fall of firing rate, but recovery seems marginal because the minimum firing rate was clipped off at zero. Following termination of the stimulus a second, oppositely directed, transient response was observed in both panels.

3.4 Discussion

To the best of our knowledge, there has not been any *in vivo* study demonstrating simple spike entrainment with AC stimulation in cerebellar PCs. E-fields applied on the cerebellar cortex are potentially affecting all cell types and cellular compartments to varying degrees. Chan *et al*. study showed that both the stellate cells and PCs are modulated by AC stimulation when the E-field is oriented along the somato-dendritic axis (Chan &

Nicholson, 1986). However, during tES, the cortical cells may experience the E-field in all directions in different strengths with respect to the extra-cranial electrode. In this study, we applied the AC stimuli in three orthogonal directions, although the current steering was not perfect, in order to demonstrate the net effect of the directionality on the network using the SS activity of the PCs as the outcome variable, which are the last order of cells in the cerebellar cortical circuitry. Furthermore, we characterized the entrainment of the PC SS activity at increasing frequencies of AC stimulation. The electrodes were placed epidurally, as opposed to attaching them on the skin as in human trials, to maximize reproducibility of the E-field strengths by eliminated the extra layers of tissue and skull.

Asamoah *et al*. raised a concern that some of the observed results could result from indirect effects of AC stimulus (Asamoah, Khatoun, & Mc Laughlin, 2019). Placing the stimulation electrode on the skin can cause peripheral stimulation and affect the cerebellar activity through secondary pathways. Epidural placement of the stimulating electrode eliminated this potential source of error also. The strong dependence of the PC modulation on the electrode orientation, where the only difference is the direction of the stimulation electrode in different trials, proves that such secondary stimulation effects did not play a role.

3.4.1 Previous Reports on Polarity of Cerebellar Modulation

Several studies have shown that the direction of the E-field relative to the cellular structures determines the polarity of the modulatory effect (Bikson et al., 2004a; Rahman et al., 2013). Computational studies further looked into how electrode placement (Bikson, Datta, Rahman, & Scaturro, 2010a) and anatomical variations (Parazzini et al., 2014) affect the field distribution. However, it is not clear what the net effect of E-fields in different

directions would be on the cerebellar cortex. While some studies in human subjects reported that observed effects differ based on the direction of the field (Galea et al., 2009; Jayaram et al., 2012) , other groups contradicted with these results (Shah, Nguyen, & Madhavan, 2013) . This discrepancy may be arising primarily from three reasons: 1) The cerebellum has a folded structure, both in rodents and primates, and the cells inside the folia are oriented differently, 2) Electric field distribution may be non-uniform at the cellular level due to inhomogeneity of tissue conductivities, 3) Inhibitory interneurons of the cerebellar cortex may have differential effects on the cerebellar output. Rahman *et al*. explained the conflicting results in these reports with computer simulations showing that due to the folded structure of the cerebellum, orientation of the PCs relative to E-field significantly varies and results in opposite polarization (Rahman, Toshev, & Bikson, 2014). In agreement to these results, our preliminary data with transcranial application of the AC stimulation had different polarities of modulation in multiunit activities (MUAs) (A. S. Asan & Sahin, 2019). In addition, E-field measurements in the rat brain demonstrated substantial deviation from an expected exponential decline as a function of depth, which was difficult to explain by methodological shortcomings alone (A. S. Asan, Gok, & Sahin, 2018; Ahmet S. Asan, Gok, & Sahin, 2019) and must be the result of inhomogeneity of the conductivities in different cortical layers.

3.4.2 SS Modulation vs. E-field Direction

Transcranial electric fields may have a unique effect on each one of the several neuron types present in the cerebellar cortex. In this regard, the cellular morphology should also be carefully considered when calculating the net effect of tES. In our study, we chose the cerebellar vermis for testing. In the vermis, parallel fibers lie mediolaterally and intersect

with the PC dendrites that ramify in the parasagittal plane. With dorsoventral AC field injection (normal to the cortex), we observed that, in 10 out of 17 PCs, the firing rate increased during anodic phases and decreased during cathodic cycles, in agreement with previous studies (Bikson et al., 2004a; L. J. Bindman et al., 1964; Chan & Nicholson, 1986; Reato, Rahman, Bikson, & Parra, 2010). However, 6 of the PCs responded to stimulation in the reversed manner, i.e. activity increased during the negative cycle and vice versa. Dendritic morphology and their orientation relative to the E-field play a significant role in determining the cellular modulation (Aspart, Remme, & Obermayer, 2018; Kronberg, Bridi, Abel, Bikson, & Parra, 2017). Even though the dendritic trees of PCs spread parasagittally in the vermis, their orientation within the parasagittal plane and their specific morphology can vary substantially, and this can be responsible for the reversed response in 6 PCs that we recorded from. One of the PCs also was unresponsive to stimulation. The lack of modulation might result from the damage to the dendrites during electrode insertion.

Applying a unidirectional E-field with transcranial electrodes is practically impossible. Rahman *et al*. showed in their computational study that with transcranial electrodes the E-field have horizontal and vertical components and the intensity of the tangential component is significantly larger than the radial component (Rahman et al., 2013). We made similar conclusions from experimental E-field data collected in rats (Ahmet S. Asan et al., 2019). Moreover, the various types of neurons located in the cerebellar cortex can respond differently to E-fields in different directions because of diversity in their size, morphology and orientation. Radial E-field causes opposite polarization of the apical dendrites and the soma while tangential component is not

expected to polarize the soma but only the synaptic efficacies (Rahman et al., 2013). Thus, the horizontal and vertical currents to the cortex may utilize different mechanisms to modulate neural activity.

We observed barely detectable levels of modulation only during some trials of ML field application. The polarization on PCs is expected to be lowest in this direction due to parasagittal orientation of the dendritic branches in the vermis. Therefore, the main modulatory effect should result either from parallel fibers (PFs), which lie parallel to the E-field, or the interneurons. Chan *et al*. paper stated that PFs are significantly less sensitive to horizontal E-fields due to their small diameters. The resting potential along the PF membrane may be affected by the E-field, but we agree that this would not be able to generate new spikes or block the existent ones at the measured E-field intensities. However, the presynaptic terminals of the parallel fibers on the PC dendrites may be polarized, in a direction that can facilitate the synaptic transmission, due to currents entering the fibers at the terminals and exiting throughout their length. This excitatory effect, however, may be balanced by the increased activity of the inhibitory cells that are also driven by the parallel fibers. Thus, it is difficult to completely exclude the E-field effects on the parallel fibers based on the results that the ML modulation was not very effective.

Rostrocaudal E-field generated significantly stronger modulation than the ML stimulation. The RC E-field is expected to polarize mostly the large dendritic tree of PCs since the bipolar E-fields decrease quickly by depth and become relatively much smaller at the level of the soma. In contrast, DV stimulation is a monopolar configuration and its E-field should reach down to the PC somas more effectively than the RC and ML E-fields. Thus, the larger modulatory effect of the RC stimulation is likely resulted from the

enhancement of the synaptic efficacies on the dendrites, rather than polarization of the soma. Hyperpolarization of the dendrites is expected to increase the modulation magnitude by increasing the EPSP (Kabakov et al., 2012). Computer models based on passive cell properties predict that cellular polarization is directly correlated with the distance between the soma and the apical dendrites. Radman *et al*. showed in a slice preparation that the larger the cortical cells are the more they are polarized by the extracellular E-field (Radman et al., 2009b) as predicted by volume conductor theory. Among the neurons in the cerebellar cortex, the PCs have the largest soma (~30μm) and soma-dendrite length, and an extensive dendritic tree. Thus, it is conceivable that the direct effect of the E-field would be the largest compared to the indirect modulation via inhibitory cells or presynaptic terminals acting on the PCs.

We tried to record from the PCs at similar depths near the surface and in the center of the round window in the electrode substrate to ensure that the E-field intensity is approximately the same for all recorded cells. Differences in modulation index observed in different cells could arise from variations of the PC position with respect to the stimulating electrodes and in cellular morphology. It was not possible to determine the threshold E-field levels for PC modulation due to spontaneous variations in the PC firing rates. The modulation index increased with increasing levels of the current injected and complete suppression of the spikes was observed in the negative cycles before a plateau effect could be seen in the firing rates during the positive cycles. Thus, the up and down modulatory effects were not symmetrical for the two halves of the AC cycle. This might have introduced a non-linear component also into the modulation index measure, which was defined as the standard deviation of the ISIs divided by their mean value.

3.4.3 Entrainment of SSs by AC

Rhythmic activity spanning a large range of frequencies has been reported for the cerebellum. For example, PC complex spikes show transient ~10 Hz as well as slower (~1Hz) rhythmicity induced via climbing fiber activity from the inferior olive (E. J. Lang, 2001; E. J. Lang, Sugihara, Welsh, & Llinás, 1999). In contrast, simple spikes and local fields can show oscillatory activity over much high frequencies, ones that can be as high as 160-240Hz (De Zeeuw, Hoebeek, & Schonewille, 2008) and they emerge in some form of phase-amplitude relation to the oscillations in the cerebrum (Courtemanche, Robinson, & Aponte, 2013; De Zeeuw et al., 2008) that suggests exchange of information. It is conceivable that the local field potential oscillations commonly observed in the cerebellum may be entrained with tACS, as demonstrated in other parts of the brain [ref]. Strengthening these cerebello-cerebral connections can potentially facilitate motor and cognitive functions, as suggested by several human studies (Alalade, Denny, Potter, Steffens, & Wang, 2011; P. Pope & Miall, 2014; Watson, Becker, Apps, & Jones, 2014). Naro *et al*. applied AC stimulation at various frequencies to the cerebellum in healthy individuals and recorded muscle potentials evoked by stimulation of the contralateral primary motor cortex (Naro et al., 2016b). They noted that 50 Hz stimulation led to reduction in the cerebello-brain inhibition (CBI) effect and facilitation of the muscle evoked potentials (MEPs). However, 10 Hz and 300 Hz resulted in mild or no effect on the CBI and MEPs. Miyaguchi *et al*. also applied AC at gamma (70 Hz) frequencies to the motor and cerebellar cortices and reported that simultaneous stimulation of these two regions improved the visuomotor performance (Miyaguchi et al., 2018). In another study,

the same group provided further evidence that the reason for this increase was the enhancement of cerebello-cerebral connections (Miyaguchi et al., 2019).

The present results show that a group of PCs can follow cycle-by-cycle AC stimulation up to 100 Hz. Some PCs were not able to track the stimulus frequency and began skipping cycles before reaching 100 Hz, which could be related to the spontaneous firing rates. There are alternating bands of zebrin+ and zebrin- across the cerebellar cortex defined by the expression of aldolase C enzyme. PCs in zebrin- zones are known to fire at about twice higher rates than those in zebrin+ bands. The PCs with high SS rates may be following the stimulus frequency up to higher rates. However, there was no correlation between the highest entrainment frequency and the spontaneous rates. Thus, we have to assume that other electrophysiological factors including the specific cerebello-cerebral connection and the functional network that the PC is a part of might have played a role in maximum entrainment frequency.

3.4.4 DC Modulation

We observed polarity dependent modulation with DC stimulation, as expected. Unlike tDCS studies in awake subjects that use ramp-up and ramp-down periods, we applied the DC with rectangular shape, and this caused drastic jumps in the PC firing rates at the onset and offset of the stimulation. The sharp change in SS firing rates indicates that the PCs have a response to fast-changing or high frequency components of the stimulus current, which is in line with the results of high frequency AC stimulation. After the initial jump, spike activity tends to return to the baseline levels with a time-constant that is on the order of 10-20s, which is in general in agreement with ramp times used in clinical studies (Marom Bikson et al., 2016a).

CHAPTER 4

MODULATION OF CEREBELLAR PURKINJE CELL ACTIVITY WITH FOCUSED ULTRASOUND STIMULATION

4.1. Objective / Background Information

Understanding the underlying mechanism of the neuromodulation methods and their influence on the central nervous system are crucial due to their ability to provide therapeutic interventions to a wide variety of neurological disorders. To this end, different physical phenomena are used to modulate the neural activity such as electricity, acoustics waves and magnetic field. Among different paradigms, ultrasound stimulation comes into prominence due to its ability of focusing and inducing reversible effects on deeper brain regions without disturbing the superficial and neighboring areas. Another key advantage of focused ultrasound stimulation (FUS) is being able to couple with the imagining techniques so that it can be used for brain mapping studies.

Although FUS has started to garner significant interest in recent years, the first applications go back to early 20th century. In 1928, Harvey conducted an *ex vivo* animal experiment showing the feasibility of peripheral nerve stimulation with ultrasound. Later, Fry *et al.* demonstrated that high intensity focused ultrasound (HIFU) can be utilized to ablate brain tissues for movement disorders and chronic pain. Steady potential shifts were also measured in the rat thalamus, hippocampus, and caudate nucleus (Koroleva, Vykhodtseva, & Elagin, 1986). Unlike these early applications, recent studies have mostly focused on the low intensity focused ultrasound and shown its modulatory effect on the neural activities. In 2008, Tyler's group reported that low-intensity FUS (LIFUS) reversibly modulated the activity in the hippocampal slice culture (Tyler et al., 2008a).

Studies on rats (King, Brown, & Pauly, 2014), mice (Tufail et al., 2010), and rabbits (Yoo et al., 2011) showed muscle contractions as a response to LIFUS when it is applied to the motor cortex. As one of the first human LIFUS applications, Hameroff and colleagues reported that targeting the posterior frontal cortex leads to enhancement in temper and suppression in pain level (Hameroff et al., 2013).

Even though this technique has been used in many different studies and showed promising outcomes, its mechanism of action is not quite understood yet. One possible explanation about its mechanism is that ultrasound waves stimulate the mechanosensitive ion-channels and allow ions to move across the membrane (Tyler et al., 2008a). Also, radiation force generated by FUS is thought to stretch the membrane bilayer and lead to changes on the instantaneous membrane capacitance which eventually manipulate the capacitive current and activate the voltage gated ion channels (Blackmore, Shrivastava, Sallet, Butler, & Cleveland, 2019). It is also hypothesized that this mechanical force causes the formation of the cavities within the cellular membrane, mediate changes on the membrane capacitance and pushes the neurons to its firing threshold (Plaksin, Shoham, & Kimmel, 2014). As an alternative theory, Oh *et al* also showed that FUS opens the Ca^{+2} channels of astrocytes and causing them to release glutamate to the extracellular space which results in increasing the overall excitability (Oh et al., 2019).

In the field of neuromodulation, there has been a growing attention for using the LIFUS as a stimulation paradigm due to its aforementioned advantages over other non-invasive stimulation techniques and also to the cerebellum as a targeted brain site because of its recently discovered roles in cognitive functions. However, studies looking into the mechanism of how LIFUS modulate the activity in the cerebellar cortex are scarce in the

literature. In this section, we aim to investigate the response of the cerebellar PCs to the LIFUS and provide insight how ultrasound modulates the single cell activity in the cerebellar cortex.

LIFUS can be applied either in continuous or pulsed manner. However, most of the studies favor the pulsed stimulation due to its higher efficacy (Kim, Chiu, Lee, Fischer, & Yoo, 2014). Therefore, in this study, we employed pulsed LIFUS as a stimulation paradigm to modulate the activity in the cerebellar cortex. There are different parameters that play role in the effectiveness of the pulsed LIFUS; however, we only focused on the pulse width and looked into how it affects the spike timing. Our results showed that LIFUS does not change the overall firing rate but the spike timing in the Purkinje cells (PCs) of the cerebellar cortex. It entrained the spike activity of the cerebellar PCs and the level of the entrainment was higher with the smaller pulse width. To the best our knowledge, this is the first study showing how LIFUS affects the single-unit activity of PCs and providing an understanding of the importance of the pulse width on neural entrainment.

4.2 Methods

4.2.1 Animal Surgery

Six Sprague Dawley rats (320-350 g) were used in this study. All procedures were approved and performed in accordance to the guidelines of the Institutional Animal Care and Use Committee (IACUC), Rutgers University, Newark, NJ. Animals were initially anesthetized with the ketamine/xylazine (80mg/kg and 12mg/kg, IP) mixture and additional doses of ketamine were injected as needed during the course of surgery. After removing the hair over the top of the head, animals were placed to the stereotaxic frame.

The blood-oxygen level (>92%) and heart rate were monitored with a pulse oximeter. Body temperature was measured by a rectal probe and regulated at 36.5ºC with a heating pad under the animal.

4.2.2 Neural Recording

An incision was made to remove the skin and muscle tissue over the dorsal part of the skull to open a craniotomy hole over the cerebellum. Then, the dura was punctured with a sharp 31g needle and cut with micro-scissors to open a small window to insert the recording electrode into the cerebellar cortex. A glass micropipette electrode with 3-5 MΩ was used as a recording electrode and slowly inserted into the cortex with the help of a 10μm step-size micromanipulator. Neural activities were recorded from either vermis 6 or 7 region of the cerebellum. A Ag/AgCl wire was attached over the skull as a recording reference electrode. Neural activity was simultaneously monitored on the oscilloscope and listened through an audio speaker while searching for the PC activity with the glass electrode inside the cerebellar cortex.

4.2.3 FUS Stimulation

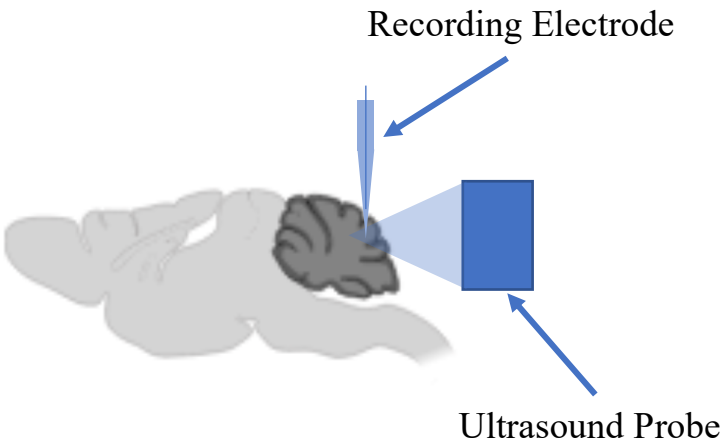

Figure 4.1 Schematic view of the placement of the recording electrode and stimulation probe.

Recording electrode was inserted into the cerebellar cortex from the anterior side while positioning the ultrasound probe at the posterior side of the cerebellum so that it can target the recording area. In order to focus the output of the ultrasound probe, a 3D printed cone with 2mm tip diameter was attached to the probe and filled with degassed saline. The tip of the cone was covered with a plastic film (<12um) and placed adjacent to the cortex. The gap between the cone and the cerebellar cortex was filled with an ultrasound gel (Aquagel, Aquasonic, MI). The length of the neural recording was kept at 10s and each second of recording contained 500 ms of ultrasound stimulation followed by 500 ms of no stimulation period. Upon the completion of the first set of neural activity, recording electrode was repositioned to obtain another set of recording.

Even though there are multiple stimulation parameters that potentially has an impact on the modulation, we only focused on investigating the effect of pulse duration.

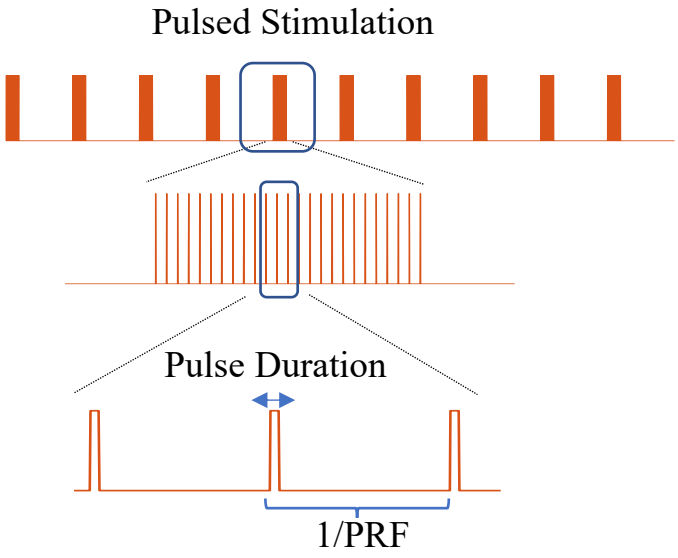

Figure 4.2 An illustration of the applied pulse stimulation.

Central frequency and pulse repetition frequency (PRF) were set to 500 kHz and 50 or 100 Hz, respectively. Skull causes significant attenuation to ultrasound, and this also makes central frequency critical for noninvasive applications. However, in this study, we do not have attenuation problem since we removed the skull over the cerebellum and applied the ultrasound directly to the cerebellar cortex. Also, 50 or 100 Hz for PRF was selected to make it close to the spontaneous firing of PCs. After identifying a PC activity, stimulation intensity was set to a relatively low level and slowly increased until seeing an entrainment on the spike activity. Once observing modulation, the length of the pulse duration was adjusted to 0.5, 1, and 2 ms respectively. The level of stimulation intensity was determined independently during each recording based on the modulation level on the PCs.

4.2.4 Data Collection and Analysis

The neural recordings were performed in a large Faraday cage through a physiological amplifier (Model 1700, modified for high-input impedance, A-M Systems, WA) with filter setting at 100Hz–5kHz by a gain of 1,000 or 10,000, depending on the spike amplitudes. Recorded signals were sampled at 100kHz through a National Instruments data acquisition board (PCI 6071) controlled via MATLAB software. Single unit activities from a total of 18 PCs were recorded in 6 animals. Spikes were detected with a peak detection algorithm which used a threshold value determined based on the signal to noise ratio. The recordings were divided into 2 sections; baseline and stimulation periods. To find the mean firing rate in these two periods, the number of spikes occurred in each section were divided by their duration, and to measure the level of entrainment, peri-event histograms of simple spikes were constructed with respect to the applied ultrasound pulse.

4.3 Results

4.3.1 Cerebellar PCs Entrainment with LIFUS

Baseline PC activity manifests an inter-spike interval (ISI) pattern with slight fluctuation in time. Once the pulsed ultrasound was applied to the cerebellar cortex, ISIs became more stable since the spike timing of the PCs started to synchronize with the ultrasound pulse. Figure 4.3 (top row) demonstrates this entrainment in an expanded time scale.

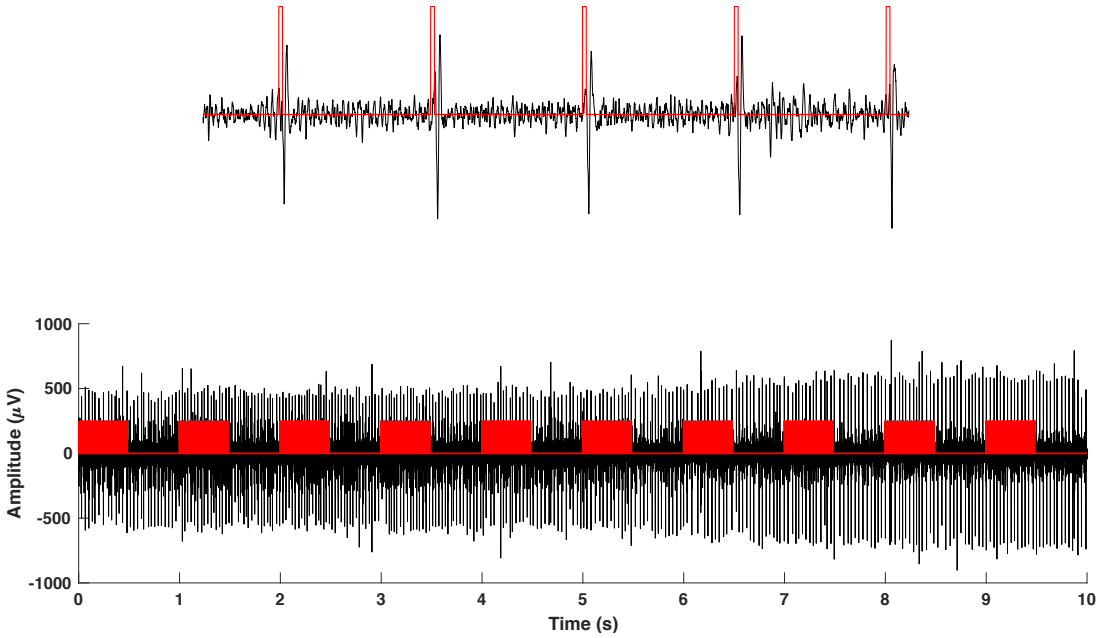

Figure 4.3 Neural recordings from a PC during LIFUS. The bottom row contains a sample recording in a long time frame while the top trace shows an episode in an expanded time scale.

Figure 4.3 (bottom row) also shows a sample PC recording during the LIFUS application shown in the red trace. The length of the neural recording was 10 s long with a train of 0.5 ms stimulation pulses turning on and off at 50 or 100 Hz. Peri-event histograms were constructed with respect to the onset times of LIFUS's pulse (Figure 4.4). Similar histograms were made for non-stimulated periods in between the stimulation trains for comparison.

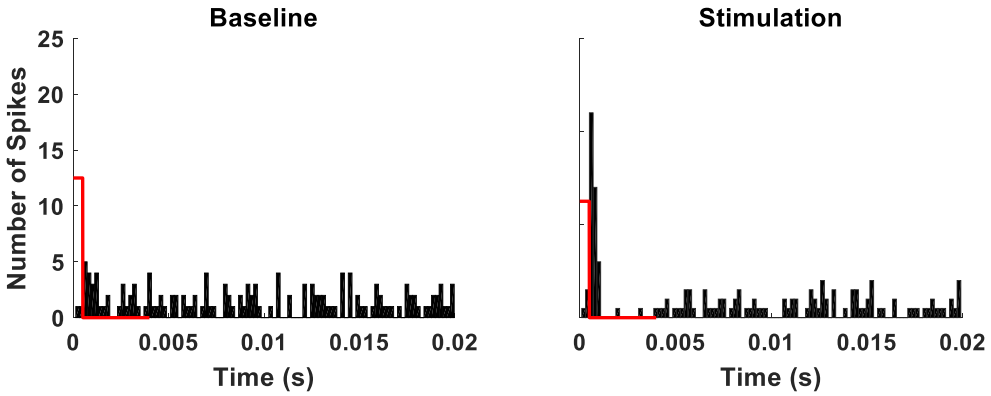

Figure 4.4 Peri-event histograms showing the number of spikes as a function of time during the baseline and stimulation periods. The red line represents the applied ultrasonic pulse, also added to the baseline plot although not applied, for comparison.

The spike activity is uniformly distributed across the 20 ms window when there is no stimulation; however, when LIFUS is applied, spikes are locked to the LIFUS pattern, and each pulse was followed by a few millisecond silence period. In order to quantify the level of entrainment, we calculated the spike occurrence rate around the pulse by dividing the number of spikes occurred during the first 10% of the pulse period to the total number of spikes. For the baseline section, we used a sliding window with 50% overlap and calculated the level of entrainment for each 10%. The maximum value among them was used for comparison. We recorded 18 PC (10 with 50Hz and 8 with 100Hz) activity during the pulse stimulation with 0.5 ms pulse width. Two-sided paired t-test results, between stimulation and baseline, showed that PCs activity modulation was significant ($p<0.02$).

We also compared the firing rate during the stimulation and baseline periods to determine if LIFUS increases the overall firing rate or simply adjusts the spike timings. Paired t-test results showed no significant difference between the average rates, which suggests that observed increase in the peri-event histogram results from redistribution of spike timings.

4.3.2 Effect of Pulse Width on the Entrainment

Reports from varying studies are suggesting that different LIFUS parameters may have a differential effect on the stimulation type and efficacy (King et al., 2013; Yoo et al., 2011). Here, we primarily focused on the pulse width to investigate its effect on the neural entrainment, and applied LIFUS to the cerebellar cortex with 0.5, 1, and 2 ms pulse widths.

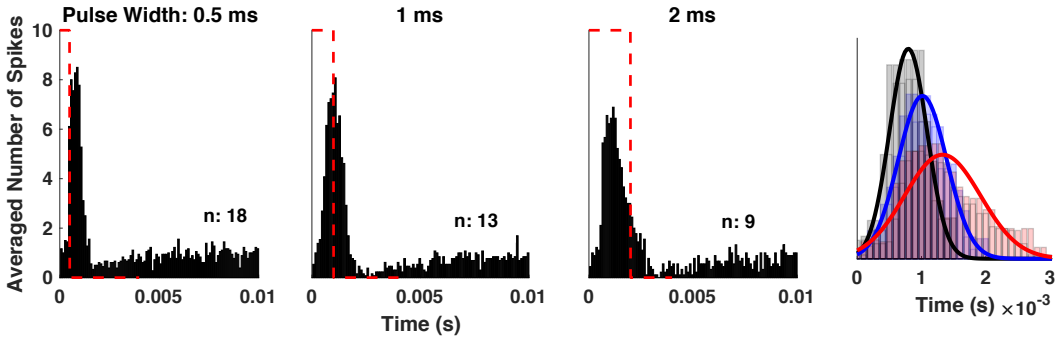

Figure 4.5 Averaged number of spikes as a function of time with 0.5, 1, and 2 ms ultrasonic pulse durations. Red dash line represents the applied pulse. The Gaussian distribution plot on the right shows the curve fit to the histogram of spike timings with respect to the applied pulse during the first 3 ms after the onset of ultrasound stimulation.

Figure 4.5 shows the average number of spikes, from multiple PCs, with respect to ultrasound pulse during 0.5, 1, and 2 ms pulse widths. The probability of spike occurrence considerably increased at LIFUS onset with a delay of less than 1 ms. The probability decreases after a peak regardless of the LIFUS duration. However, the longer ultrasound pulses (1 ms and 2 ms) had a wider spread of spike timings as shown in the averaged plots and the Gaussian curve fits on the right. The high probability window was followed by a reduced probability interval that seems to last longer with longer LIFUS durations. Then, the spike probability recovered to that of the unstimulated periods.

4.4 Discussion

The effects of FUS on different part of the central nervous system have been reported, however, the cerebellum was never tested in these reports. We believe that the cerebellum is an ideal target for FUS studies due to its unique anatomical structure and the diversity of functions that it is involved in. The cerebellar modulation has the potential to enhance both motor and cognitive functions, which makes it a crucial target for the treatment of a wide variety of neurological disorders. Even though the deep cerebellar nuclei (DCN) are the final pathway from the cerebellum, the PCs, located near the cortical surface, are responsible to sculpt the activity in the DCN. This allows modulation of the cerebellar output by stimulation of the cerebellar cortex, a more superficial and easier target than the DCN. In this respect, we selected the cerebellar cortex as a target to investigate how FUS modulate the neural activity in the cerebellum, and how to optimize modulation specifically by varying the FUS pulse width.

4.4.1 Central Frequency

In order to have an effective stimulation, the sonication parameters should be carefully determined. Central frequency is one of the FUS parameters that is crucial when targeting the smaller areas since it directly defines the ultrasonic beam size. For transcranial applications, it is not possible to use frequencies above 1 MHz because high frequencies are scattered by the skull and cannot be focused into the brain. In order to overcome this obstacle, some studies applied ultrasound with comparable low frequencies, but from multiple sources that provided a smaller focus area in their intersection (Jolesz, 2009; Mehić et al., 2014). However, overall, if one wants to stimulate a cortical area smaller than 1 mm diameter, the central frequency has to be above 600 kHz (Lee et al., 2018). In this

study, we utilized 500 kHz as the central frequency. Although we do not have an attenuation problem of the skull in this acute preparation, we used a relatively lower frequency because we wanted to apply the FUS to a larger area and investigate its impact on the overall activity in the cerebellar cortex.

4.4.2 Acoustic Intensity

Acoustic intensity level was attributed to the level of excitation since it determines the magnitude of the applied radiation force. In this study, we adjusted the intensity level based on the cellular response. PC activity is sensitive to mechanical perturbations. Therefore, it is difficult to keep the activity of a neuron for a long time especially at high intensity levels of the FUS. Hence, we started the testing with low intensities of ultrasonic stimulation where we did not observe modulation, and then slowly increased the intensity until detecting a modulation in the PCs. We were not able to record the activity of PCs closer to the cerebellar cortex since they are more sensitive to the mechanical disturbance (dimpling) of the pia by penetration of the recording electrode. Hence, most of our recordings were made from 2-3 mm depths from the cortical surface. It should also be noted that positioning the FUS probe properly for maximum modulatory effect was not easy and even possible in some cases. It seems that there is a small 'sweet spot' where the reported effects in this study can be observed. The relative positioning of the cell within the ultrasonic beam to achieve the best effect is not very clear at this point. PCs have a spontaneous firing rate around 50 Hz (Van Dijck et al., 2013). The pulse repetition frequency (PRF) was chosen in the same ballpark range, 50 or 100 Hz, to the PC firing rates on average. Then, we measured the level of entrainment during application of different pulsed widths.

4.4.3 Entrainment

To the best of our knowledge, there is only one study employed ultrasound to stimulate the cerebellum. In that study, the authors employed a stroke mouse model and stimulated the lateral cerebellar nucleus while recording the motor evoked potentials (Baek, Pahk, Kim, Youn, & Kim, 2018). They reported that animals exposed to LIFUS have significantly better somatosensory recovery than the control group.

Our study is the first report showing the effect of FUS at a single cell level in the cerebellar cortex. We applied ultrasound stimulation with different pulse widths and simultaneously recorded the extracellular single unit activity of the PCs to probe how this newly developed method modulates the spike activity in the cerebellar cortex. Our results showed that the single unit activity of the PCs is effectively entrained by the ultrasound, and the level of entrainment is stronger with shorter pulse widths.

4.4.4 Mechanism

FUS is divided into two categories based on the applied acoustic intensity level; this also defines the mechanism that is utilized to modulate the neural activity. High intensity ultrasound stimulation causes temperature elevation (Clarke & ter Haar, 1997), which in turn suppresses the neural activity, and causes cavitation. Hence, it is not considered safe and mostly used for surgical applications such as tissue ablation (ter Haar, 1999). On the other hand, LIFUS reversibly modulate the neural activity without causing any damage.

Different hypotheses were developed to clarify the underlying mechanism of LIFUS. Tyler *et al*. showed that LIFUS modulate neurons by triggering the voltage gated ion channels (Tyler et al., 2008a). Oh *et al.*, on the other hand, demonstrated that LIFUS stimulates Ca^{+2} channels of astrocytes resulting in the glutamate release to the extracellular

environment, thereby elevating overall excitability. Modifying the neurotransmitter level in the extracellular space can explain the observed after-effects subsequent to FUS. Even though it is not expected to see the cavitation as a result of low intensity applications, Krasovitski *et al.* showed in their studies that LIFUS generates nano-cavities within the cellular membrane and alters the membrane capacitance which drives the cell toward its firing threshold (Krasovitski, Frenkel, Shoham, & Kimmel, 2011).

There are some discrepancies in the published studies which need to be resolved for better interpretation of the effects of stimulation. Kings *et al.* demonstrated that continuous ultrasound is more effective than the pulsed stimulation (King et al., 2013). This study was supported by data from Plaksin *et al.* while opposed by others (Kim et al., 2015; Yoo et al., 2011). In another study, Plaksin *et al.* also suggested that ion channels may have a differential response to the applied stimulation shape, and they demonstrated that T-type voltage gated calcium channels are more sensitive to short pulse widths (Plaksin, Kimmel, & Shoham, 2016). This report also addresses the potential reason for the aforementioned contradiction and pinpoints another cellular mechanism involved in determining the cellular response, i.e. ion channel selectivity.

Even though the modulatory effect of FUS is mostly attributed to the excitatory mechanisms, Yoo *et al*. and Kim *et al*. also reported the inhibitory effect of FUS in the visual cortex (Kim et al., 2015; Yoo et al., 2011). The source of this discrepancy may arise from the affected neuron type since the inhibitory effect can be mediated by either excitation of the inhibitory neurons, or inhibition of the excitatory neurons.

In our study we observed that short pulse duration is more effective for neural entrainment. The proposed mechanism by Plaksin, which suggests that short pulses

stimulate T-type Ca^{+2} channels, agrees with our findings since T-types channels are abundant in the cerebellar PCs (Isope & Murphy, 2005), and this could be one of the mechanisms.

Another possible explanation for our finding is that the probability of producing a simple spike is reduced during an interval as a rebound effect at the offset of the FUS. If the ultrasonic stimulus is turned off early (at 0.5ms), this sharpens the histogram by starting the lowered-probability-of-firing interval earlier. If the ultrasonic stimulation is kept on for 1 ms or 2 ms, the entrainment continues with heightened but decreasing firing probabilities for another millisecond after the onset of the ultrasonic stimulation. However, the shift and reduction of the peak probability with increasing FUS durations can only be explained by the fact that the probability of firing is somewhat less than the baseline level even at the time the next FUS pulse is delivered 10 or 20 ms later. That is, when the next stimulus comes in, the probability of firing is somewhat less, and the delay is larger with longer FUS pulses that contain more power. Thus, there must be inhibitory effects of FUS that last at least for 10-20 ms. The inhibitory effect is stronger with longer FUS pulse durations because they contain more power.

Shorter pulse widths are more effective on PCs due to presence of the T-Type channels and this effect decays with the increased pulse width. However, if the inhibitory cells of the cerebellar are also excited, this effect is expected to be directly correlated with the pulse width because longer pulse carry more power. Since interneurons play a role in adjusting the activity pattern of the PCs at a longer time scale (Brown et al., 2019), their activation potentially changes the spike timing of PCs and results in relatively elevated irregular activity observed as wider bell-shaped spike distribution. Thus, the activation of

interneurons may be the mechanism underlying the differences in the histograms for the short and long FUS pulses.

CHAPTER 5

CONCLUSION / SUMMARY

Traditionally, the cerebellum has been considered as a brain center for sensorimotor integration and motor coordination. In recent years the cerebellum has also been implicated in cognitive functions and emotions. Due to its involvement in varying tasks, any impairment in the cerebellar circuitry can cause manifold neurological disorders associated with cognitive and motor functions. In this respect, neuromodulation methods come into play and offer treatment to those who suffer from cerebellar disorders. tES, TMS and FUS are some of the promising methods that are non-invasive and easy to apply clinically. However, there are still open questions need to be answered about how these methods change the activity pattern in the cerebellum. Animal studies offer an ample platform to further probe the underlying mechanism of these methods. To this end, in this study, we used an animal model to investigate how electric fields and ultrasound stimulation modulate the activity in the cerebellar cortex.

The magnitude and direction of the electric field is the main parameter that determines the efficacy of the electrical currents applied to neural tissue. Therefore, as an initial step, we looked into how the e-field is distributed in the brain since this can help us better interpret/understand the effects of electric stimulation on neuronal structures. Our findings demonstrated that e-field decays exponentially, and skin shunts most of the e-field. Over-the-skull-placement of the stimulation electrode seems ideal since it is not as invasive as intracranial placement, and its effectiveness is significantly better than over-the-skin stimulation. On the other hand, placing the return electrode at different extracephalic positions does not affect the e-field distribution.

As a second step, we employed two most common types of the electrical stimulation methods, tDCS and tACS, and showed how they modulate the activity in the cerebellar cortex. In this study, we applied electric stimulation in different orientations to the cerebellar cortex to investigate which direction generates a stronger modulatory effect on the Purkinje cells of the cerebellar cortex. Our results showed that the rostrocaudal e-field injection generates a higher modulation level. We also observed that AC stimulation with low frequencies cause burst like activity while high frequencies lead to locking between the stimulation cycles and spikes. This high frequency response is also aligned with our DC stimulation results where we observed a sharp response at the onset and offset of the stimulation current.

In the last part, we investigated the modulatory effect of the ultrasound stimulation on the cerebellar cortex. Ultrasound stimulation is a promising modulation method, however; its mechanism of action is not well understood yet. Here, we presented how it entrains the single unit activity of the cerebellar PCs. Our results showed that FUS does not change the number of spikes but modify their timings, and shorter pulse widths generate stronger locking with the spikes.

To summarize, this thesis develops a novel understanding of how the activity in the cerebellar cortex is modulated by electric and ultrasound stimulation. The results of this study can help the development of more effective non-invasive cerebellar stimulation procedures in the clinic.

REFERENCES

Alalade, E., Denny, K., Potter, G., Steffens, D., & Wang, L. (2011). Altered Cerebellar-Cerebral Functional Connectivity in Geriatric Depression. *PLOS ONE, 6*(5), e20035. doi:10.1371/journal.pone.0020035

Antal, A., Alekseichuk, I., Bikson, M., Brockmoller, J., Brunoni, A. R., Chen, R., . . . Paulus, W. (2017). Low intensity transcranial electric stimulation: Safety, ethical, legal regulatory and application guidelines. *Clinical neurophysiology : official journal of the International Federation of Clinical Neurophysiology, 128*(9), 1774-1809. doi:10.1016/j.clinph.2017.06.001

Antal, A., Alekseichuk, I., Bikson, M., Brockmöller, J., Brunoni, A. R., Chen, R., . . . Paulus, W. (2017). Low intensity transcranial electric stimulation: Safety, ethical, legal regulatory and application guidelines. *Clinical Neurophysiology, 128*(9), 1774-1809. doi:https://doi.org/10.1016/j.clinph.2017.06.001

Asamoah, B., Khatoun, A., & Mc Laughlin, M. (2019). tACS motor system effects can be caused by transcutaneous stimulation of peripheral nerves. *Nature Communications, 10*(1), 266. doi:10.1038/s41467-018-08183-w

Asan, A. S., Gok, S., & Sahin, M. (2018, 18-21 July 2018). *Electric Fields Induced By Transcutaneous And Intracranial Current Injections In The Rat Brain.* Paper presented at the 2018 40th Annual International Conference of the IEEE Engineering in Medicine and Biology Society (EMBC).

Asan, A. S., Gok, S., & Sahin, M. (2019). Electrical fields induced inside the rat brain with skin, skull, and dural placements of the current injection electrode. *PLOS ONE, 14*(1), e0203727. doi:10.1371/journal.pone.0203727

Asan, A. S., & Sahin, M. (2019, 23-27 July 2019). *Modulation of Multiunit Spike Activity by Transcranial AC Stimulation (tACS) in the Rat Cerebellar Cortex.* Paper presented at the 2019 41st Annual International Conference of the IEEE Engineering in Medicine and Biology Society (EMBC).

Aspart, F., Remme, M. W. H., & Obermayer, K. (2018). Differential polarization of cortical pyramidal neuron dendrites through weak extracellular fields. *PLOS Computational Biology, 14*(5), e1006124. doi:10.1371/journal.pcbi.1006124

Baek, H., Pahk, K. J., Kim, M.-J., Youn, I., & Kim, H. (2018). Modulation of Cerebellar Cortical Plasticity Using Low-Intensity Focused Ultrasound for Poststroke Sensorimotor Function Recovery. *Neurorehabilitation and Neural Repair, 32*(9), 777-787. doi:10.1177/1545968318790022

Bais, M., Figee, M., & Denys, D. (2014). Neuromodulation in Obsessive-Compulsive Disorder. *Psychiatric Clinics of North America, 37*(3), 393-413. doi:https://doi.org/10.1016/j.psc.2014.06.003

Bikson, M., Datta, A., Rahman, A., & Scaturro, J. (2010a). Electrode montages for tDCS and weak transcranial electrical stimulation: role of "return" electrode's position and size. *Clinical neurophysiology : official journal of the International Federation of Clinical Neurophysiology, 121*(12), 1976-1978. doi:10.1016/j.clinph.2010.05.020

Bikson, M., Datta, A., Rahman, A., & Scaturro, J. (2010b). Electrode montages for tDCS and weak transcranial electrical stimulation: Role of "return" electrode's position and size. *Clinical Neurophysiology, 121*(12), 1976-1978. doi:https://doi.org/10.1016/j.clinph.2010.05.020

Bikson, M., Grossman, P., Thomas, C., Zannou, A. L., Jiang, J., Adnan, T., . . . Woods, A. J. (2016a). Safety of Transcranial Direct Current Stimulation: Evidence Based Update 2016. *Brain Stimulation, 9*(5), 641-661. doi:https://doi.org/10.1016/j.brs.2016.06.004

Bikson, M., Grossman, P., Thomas, C., Zannou, A. L., Jiang, J., Adnan, T., . . . Woods, A. J. (2016). Safety of Transcranial Direct Current Stimulation: Evidence Based Update 2016. *Brain Stimul, 9*(5), 641-661. doi:10.1016/j.brs.2016.06.004

Bikson, M., Grossman, P., Thomas, C., Zannou, A. L., Jiang, J., Adnan, T., . . . Woods, A. J. (2016b). Safety of Transcranial Direct Current Stimulation: Evidence Based Update 2016. *Brain Stimulation: Basic, Translational, and Clinical Research in Neuromodulation, 9*(5), 641-661. doi:10.1016/j.brs.2016.06.004

Bikson, M., Inoue, M., Akiyama, H., Deans, J. K., Fox, J. E., Miyakawa, H., & Jefferys, J. G. R. (2004a). Effects of uniform extracellular DC electric fields on excitability in rat hippocampal slices in vitro. *The Journal of physiology, 557*(1), 175-190. doi:10.1113/jphysiol.2003.055772

Bikson, M., Inoue, M., Akiyama, H., Deans, J. K., Fox, J. E., Miyakawa, H., & Jefferys, J. G. R. (2004b). Effects of uniform extracellular DC electric fields on excitability in rat hippocampal slices in vitro. *The Journal of physiology, 557*(Pt 1), 175-190. doi:10.1113/jphysiol.2003.055772

Bikson, M., Paulus, W., Esmaeilpour, Z., Kronberg, G., & Nitsche, M. A. (2019). Mechanisms of Acute and After Effects of Transcranial Direct Current Stimulation. In H. Knotkova, M. A. Nitsche, M. Bikson, & A. J. Woods (Eds.), *Practical Guide to Transcranial Direct Current Stimulation: Principles, Procedures and Applications* (pp. 81-113). Cham: Springer International Publishing.

Bindman, L. J., Lippold, O. C., & Redfearn, J. W. (1964). The Action Of Brief Polarizing Currents On The Cerebral Cortex Of The Rat (1) During Current Flow And (2) In The Production Of Long-Lasting After-Effects. *The Journal of physiology, 172*(3), 369-382. doi:10.1113/jphysiol.1964.sp007425

Bindman, L. J., Lippold, O. C. J., & Redfearn, J. W. T. (1964). The action of brief polarizing currents on the cerebral cortex of the rat (1) during current flow and (2) in the production of long-lasting after-effects. *The Journal of physiology, 172*(3), 369-382. doi:10.1113/jphysiol.1964.sp007425

Blackmore, J., Shrivastava, S., Sallet, J., Butler, C. R., & Cleveland, R. O. (2019). Ultrasound Neuromodulation: A Review of Results, Mechanisms and Safety. *Ultrasound in Medicine & Biology, 45*(7), 1509-1536. doi:https://doi.org/10.1016/j.ultrasmedbio.2018.12.015

Blenkinsop, T. A., & Lang, E. J. (2011). Synaptic action of the olivocerebellar system on cerebellar nuclear spike activity. *The Journal of neuroscience : the official journal of the Society for Neuroscience, 31*(41), 14708-14720. doi:10.1523/JNEUROSCI.3323-11.2011

Block, H., & Celnik, P. (2013). Stimulating the cerebellum affects visuomotor adaptation but not intermanual transfer of learning. *Cerebellum (London, England), 12*(6), 781-793. doi:10.1007/s12311-013-0486-7

Booth, J. R., Wood, L., Lu, D., Houk, J. C., & Bitan, T. (2007). The role of the basal ganglia and cerebellum in language processing. *Brain research, 1133*(1), 136-144. doi:10.1016/j.brainres.2006.11.074

Brown, A. M., Arancillo, M., Lin, T., Catt, D. R., Zhou, J., Lackey, E. P., . . . Sillitoe, R. V. (2019). Molecular layer interneurons shape the spike activity of cerebellar Purkinje cells. *Scientific Reports, 9*(1), 1742-1742. doi:10.1038/s41598-018-38264-1

Buckner, Randy L. (2013). The Cerebellum and Cognitive Function: 25 Years of Insight from Anatomy and Neuroimaging. *Neuron, 80*(3), 807-815. doi:https://doi.org/10.1016/j.neuron.2013.10.044

Buzsáki, G., & Draguhn, A. (2004). Neuronal Oscillations in Cortical Networks. *Science, 304*(5679), 1926. doi:10.1126/science.1099745

Bystritsky, A., Korb, A. S., Douglas, P. K., Cohen, M. S., Melega, W. P., Mulgaonkar, A. P., . . . Yoo, S.-S. (2011). A review of low-intensity focused ultrasound pulsation. *Brain Stimulation: Basic, Translational, and Clinical Research in Neuromodulation, 4*(3), 125-136. doi:10.1016/j.brs.2011.03.007

Cantrell, D. R., Inayat, S., Taflove, A., Ruoff, R. S., & Troy, J. B. (2007). Incorporation of the electrode–electrolyte interface into finite-element models of metal microelectrodes. *Journal of Neural Engineering, 5*(1), 54-67. doi:10.1088/1741-2560/5/1/006

Chan, C. Y., Hounsgaard, J., & Midtgaard, J. (1989). Excitatory synaptic responses in turtle cerebellar Purkinje cells. *The Journal of physiology, 409*(1), 143-156. doi:10.1113/jphysiol.1989.sp017489

Chan, C. Y., Hounsgaard, J., & Nicholson, C. (1988). Effects of electric fields on transmembrane potential and excitability of turtle cerebellar Purkinje cells in vitro. *The Journal of physiology, 402*, 751-771. doi:10.1113/jphysiol.1988.sp017232

Chan, C. Y., & Nicholson, C. (1986). Modulation by applied electric fields of Purkinje and stellate cell activity in the isolated turtle cerebellum. *The Journal of physiology, 371*, 89-114. doi:10.1113/jphysiol.1986.sp015963

Chhatbar, P. Y., Chen, R., Deardorff, R., Dellenbach, B., Kautz, S. A., George, M. S., & Feng, W. (2017). Safety and tolerability of transcranial direct current stimulation to stroke patients – A phase I current escalation study. *Brain Stimulation, 10*(3), 553-559. doi:https://doi.org/10.1016/j.brs.2017.02.007

Clarke, R. L., & ter Haar, G. R. (1997). Temperature rise recorded during lesion formation by high-intensity focused ultrasound. *Ultrasound in Medicine and Biology, 23*(2), 299-306. doi:10.1016/S0301-5629(96)00198-6

Courtemanche, R., Robinson, J. C., & Aponte, D. I. (2013). Linking oscillations in cerebellar circuits. *Frontiers in neural circuits, 7*, 125-125. doi:10.3389/fncir.2013.00125

Creutzfeldt, O. D., Fromm, G. H., & Kapp, H. (1962). Influence of transcortical d-c currents on cortical neuronal activity. *Experimental Neurology, 5*(6), 436-452. doi:https://doi.org/10.1016/0014-4886(62)90056-0

D'Angelo, E., & Casali, S. (2013). Seeking a unified framework for cerebellar function and dysfunction: from circuit operations to cognition. *Frontiers in Neural Circuits, 6*(116). doi:10.3389/fncir.2012.00116

Datta, A., Bansal, V., Diaz, J., Patel, J., Reato, D., & Bikson, M. (2009). Gyri-precise head model of transcranial direct current stimulation: Improved spatial focality using a ring electrode versus conventional rectangular pad. *Brain Stimulation, 2*(4), 201-207.e201. doi:https://doi.org/10.1016/j.brs.2009.03.005

Datta, A., Bikson, M., & Fregni, F. (2010). Transcranial direct current stimulation in patients with skull defects and skull plates: high-resolution computational FEM study of factors altering cortical current flow. *NeuroImage, 52*(4), 1268-1278. doi:10.1016/j.neuroimage.2010.04.252

Datta, A., Elwassif, M., Battaglia, F., & Bikson, M. (2008). Transcranial current stimulation focality using disc and ring electrode configurations: FEM analysis. *Journal of Neural Engineering, 5*(2), 163-174. doi:10.1088/1741-2560/5/2/007

De Schutter, E., & Steuber, V. (2009). Patterns and pauses in Purkinje cell simple spike trains: experiments, modeling and theory. *Neuroscience, 162*(3), 816-826. doi:https://doi.org/10.1016/j.neuroscience.2009.02.040

De Zeeuw, C. I., Hoebeek, F. E., Bosman, L. W. J., Schonewille, M., Witter, L., & Koekkoek, S. K. (2011). Spatiotemporal firing patterns in the cerebellum. *Nature Reviews Neuroscience, 12*(6), 327-344. doi:10.1038/nrn3011

De Zeeuw, C. I., Hoebeek, F. E., & Schonewille, M. (2008). Causes and Consequences of Oscillations in the Cerebellar Cortex. *Neuron, 58*(5), 655-658. doi:https://doi.org/10.1016/j.neuron.2008.05.019

Dedoncker, J. G. E., Brunoni, A. R., Baeken, C. G. E. U., & Vanderhasselt, M.-A. G. E. P. P. (2016). A systematic review and meta-analysis of the effects of transcranial direct current stimulation (tDCS) over the dorsolateral prefrontal cortex in healthy and neuropsychiatric samples : influence of stimulation parameters. *(2016) BRAIN STIMULATION*. Retrieved from http://lib.ugent.be/catalog/pug01:7206618

Dockery, C. A., Liebetanz, D., Birbaumer, N., Malinowska, M., & Wesierska, M. J. (2011). Cumulative benefits of frontal transcranial direct current stimulation on visuospatial working memory training and skill learning in rats. *Neurobiology of Learning and Memory, 96*(3), 452-460. doi:https://doi.org/10.1016/j.nlm.2011.06.018

Fitzgerald, P. J., & Watson, B. O. (2018). Gamma oscillations as a biomarker for major depression: an emerging topic. *Translational psychiatry, 8*(1), 177-177. doi:10.1038/s41398-018-0239-y

Fröhlich, F., & McCormick, D. A. (2010). Endogenous electric fields may guide neocortical network activity. *Neuron, 67*(1), 129-143. doi:10.1016/j.neuron.2010.06.005

Fry, F. J., Ades, H. W., & Fry, W. J. (1958). Production of Reversible Changes in the Central Nervous System by Ultrasound. *Science, 127*(3289), 83. doi:10.1126/science.127.3289.83

Fry, W. J., Fry, F. J., Barnard, J. W., Krumins, R. F., & Brennan, J. F. (1955). Ultrasonic Lesions in the Mammalian Central Nervous System. *Science, 122*(3168), 517. doi:10.1126/science.122.3168.517

Fry, W. J., Mosberg, W. H., Barnard, J. W., & Fry, F. J. (1954). Production of Focal Destructive Lesions in the Central Nervous System With Ultrasound. *Journal of Neurosurgery, 11*(5), 471-478. doi:10.3171/jns.1954.11.5.0471

Galea, J. M., Jayaram, G., Ajagbe, L., & Celnik, P. (2009). Modulation of cerebellar excitability by polarity-specific noninvasive direct current stimulation. *The Journal of neuroscience : the official journal of the Society for Neuroscience, 29*(28), 9115-9122. doi:10.1523/JNEUROSCI.2184-09.2009

Gasca, F., Marshall, L., Binder, S., Schlaefer, A., Hofmann, U. G., & Schweikard, A. (2011, 27 April-1 May 2011). *Finite element simulation of transcranial current stimulation in realistic rat head model.* Paper presented at the 2011 5th International IEEE/EMBS Conference on Neural Engineering.

Hameroff, S., Trakas, M., Duffield, C., Annabi, E., Gerace, M. B., Boyle, P., . . . Badal, J. J. (2013). Transcranial Ultrasound (TUS) Effects on Mental States: A Pilot Study. *Brain Stimulation: Basic, Translational, and Clinical Research in Neuromodulation, 6*(3), 409-415. doi:10.1016/j.brs.2012.05.002

Hardwick, R. M., & Celnik, P. A. (2014). Cerebellar direct current stimulation enhances motor learning in older adults. *Neurobiology of aging, 35*(10), 2217-2221. doi:10.1016/j.neurobiolaging.2014.03.030

Harvey, E. N. (1929). The Effect Of High Frequency Sound Waves On Heart Muscle And Other Irritable Tissues. *American Journal of Physiology-Legacy Content, 91*(1), 284-290. doi:10.1152/ajplegacy.1929.91.1.284

Hayes, K. J. (1950). The Current Path In Electric Convulsion Shock. *Archives of Neurology & Psychiatry, 63*(1), 102-109. doi:10.1001/archneurpsyc.1950.02310190108008

Helfrich, Randolph F., Schneider, Till R., Rach, S., Trautmann-Lengsfeld, Sina A., Engel, Andreas K., & Herrmann, Christoph S. (2014). Entrainment of Brain Oscillations by Transcranial Alternating Current Stimulation. *Current Biology, 24*(3), 333-339. doi:https://doi.org/10.1016/j.cub.2013.12.041

Henry, R., Deckert, M., Guruviah, V., & Schmidt, B. (2016). Review of Neuromodulation Techniques and Technological Limitations. *IETE Technical Review, 33*(4), 368-377. doi:10.1080/02564602.2015.1106926

Herculano-Houzel, S. (2009). The human brain in numbers: a linearly scaled-up primate brain. *Frontiers in Human Neuroscience, 3*(31). doi:10.3389/neuro.09.031.2009

Herrmann, C. S., Rach, S., Neuling, T., & Strüber, D. (2013). Transcranial alternating current stimulation: a review of the underlying mechanisms and modulation of cognitive processes. *Frontiers in Human Neuroscience, 7*, 279-279. doi:10.3389/fnhum.2013.00279

Huang, Y., Liu, A. A., Lafon, B., Friedman, D., Dayan, M., Wang, X., . . . Parra, L. C. (2017). Measurements and models of electric fields in the in vivo human brain during transcranial electric stimulation. *eLife, 6*, e18834. doi:10.7554/eLife.18834

Isope, P., & Murphy, T. H. (2005). Low threshold calcium currents in rat cerebellar Purkinje cell dendritic spines are mediated by T-type calcium channels. *The Journal of physiology, 562*(Pt 1), 257-269. doi:10.1113/jphysiol.2004.074211

Jackson, M. P., Rahman, A., Lafon, B., Kronberg, G., Ling, D., Parra, L. C., & Bikson, M. (2016). Animal models of transcranial direct current stimulation: Methods and mechanisms. *Clinical Neurophysiology, 127*(11), 3425-3454. doi:https://doi.org/10.1016/j.clinph.2016.08.016

Jayaram, G., Tang, B., Pallegadda, R., Vasudevan, E. V. L., Celnik, P., & Bastian, A. (2012). Modulating locomotor adaptation with cerebellar stimulation. *Journal of neurophysiology, 107*(11), 2950-2957. doi:10.1152/jn.00645.2011

Jolesz, F. A. (2009). MRI-guided focused ultrasound surgery. *Annual review of medicine, 60*, 417-430. doi:10.1146/annurev.med.60.041707.170303

Kabakov, A. Y., Muller, P. A., Pascual-Leone, A., Jensen, F. E., & Rotenberg, A. (2012). Contribution of axonal orientation to pathway-dependent modulation of excitatory transmission by direct current stimulation in isolated rat hippocampus. *Journal of Neurophysiology, 107*(7), 1881-1889. doi:10.1152/jn.00715.2011

Kasten, F. H., Dowsett, J., & Herrmann, C. S. (2016). Sustained Aftereffect of α-tACS Lasts Up to 70 min after Stimulation. *Frontiers in Human Neuroscience, 10*(245). doi:10.3389/fnhum.2016.00245

Kim, H., Chiu, A., Lee, S. D., Fischer, K., & Yoo, S.-S. (2014). Focused ultrasound-mediated non-invasive brain stimulation: examination of sonication parameters. *Brain stimulation, 7*(5), 748-756. doi:10.1016/j.brs.2014.06.011

Kim, H., Park, M. Y., Lee, S. D., Lee, W., Chiu, A., & Yoo, S.-S. (2015). Suppression of EEG visual-evoked potentials in rats through neuromodulatory focused ultrasound. *Neuroreport, 26*(4), 211-215. doi:10.1097/WNR.0000000000000330

King, R. L., Brown, J. R., Newsome, W. T., & Pauly, K. B. (2013). Effective Parameters for Ultrasound-Induced In Vivo Neurostimulation. *Ultrasound in Medicine and Biology, 39*(2), 312-331. doi:10.1016/j.ultrasmedbio.2012.09.009

King, R. L., Brown, J. R., & Pauly, K. B. (2014). Localization of Ultrasound-Induced Neurostimulation in the Mouse Model. *Ultrasound in Medicine and Biology, 40*(7), 1512-1522. doi:10.1016/j.ultrasmedbio.2014.01.020

Knyazev, G. G. (2007). Motivation, emotion, and their inhibitory control mirrored in brain oscillations. *Neuroscience & Biobehavioral Reviews, 31*(3), 377-395. doi:https://doi.org/10.1016/j.neubiorev.2006.10.004

Koroleva, V. I., Vykhodtseva, N. I., & Elagin, V. A. (1986). Cortical and subcortical spreading depression in rats produced by focused ultrasound. *Neurophysiology, 18*(1), 43-48. doi:10.1007/BF01052490

Krasovitski, B., Frenkel, V., Shoham, S., & Kimmel, E. (2011). Intramembrane cavitation as a unifying mechanism for ultrasound-induced bioeffects. *Proceedings of the National Academy of Sciences of the United States of America, 108*(8), 3258-3263. doi:10.1073/pnas.1015771108

Krause, M. R., Vieira, P. G., Csorba, B. A., Pilly, P. K., & Pack, C. C. (2019). Transcranial alternating current stimulation entrains single-neuron activity in the primate brain. *Proceedings of the National Academy of Sciences, 116*(12), 5747. doi:10.1073/pnas.1815958116

Kronberg, G., Bridi, M., Abel, T., Bikson, M., & Parra, L. C. (2017). Direct Current Stimulation Modulates LTP and LTD: Activity Dependence and Dendritic Effects. *Brain Stimulation, 10*(1), 51-58. doi:10.1016/j.brs.2016.10.001

Lang, E. J. (2001). Organization of Olivocerebellar Activity in the Absence of Excitatory Glutamatergic Input. *The Journal of Neuroscience, 21*(5), 1663. doi:10.1523/JNEUROSCI.21-05-01663.2001

Lang, E. J., Sugihara, I., Welsh, J. P., & Llinás, R. (1999). Patterns of Spontaneous Purkinje Cell Complex Spike Activity in the Awake Rat. *The Journal of Neuroscience, 19*(7), 2728. doi:10.1523/JNEUROSCI.19-07-02728.1999

Lang, N., Siebner, H. R., Ward, N. S., Lee, L., Nitsche, M. A., Paulus, W., . . . Frackowiak, R. S. (2005). How does transcranial DC stimulation of the primary motor cortex alter regional neuronal activity in the human brain? *European Journal of Neuroscience, 22*(2), 495-504. doi:10.1111/j.1460-9568.2005.04233.x

Lee, W., Croce, P., Margolin, R. W., Cammalleri, A., Yoon, K., & Yoo, S.-S. (2018). Transcranial focused ultrasound stimulation of motor cortical areas in freely-moving awake rats. *BMC neuroscience, 19*(1), 57-57. doi:10.1186/s12868-018-0459-3

Lee, W., Kim, H., Jung, Y., Song, I.-U., Chung, Y. A., & Yoo, S.-S. (2015). Image-Guided Transcranial Focused Ultrasound Stimulates Human Primary Somatosensory Cortex. *Scientific Reports, 5*(1), 8743. doi:10.1038/srep08743

Lenartowicz, A., Mazaheri, A., Jensen, O., & Loo, S. K. (2018). Aberrant Modulation of Brain Oscillatory Activity and Attentional Impairment in Attention-Deficit/Hyperactivity Disorder. *Biological psychiatry. Cognitive neuroscience and neuroimaging, 3*(1), 19-29. doi:10.1016/j.bpsc.2017.09.009

Liebetanz, D., Koch, R., Mayenfels, S., König, F., Paulus, W., & Nitsche, M. A. (2009). Safety limits of cathodal transcranial direct current stimulation in rats. *Clinical Neurophysiology, 120*(6), 1161-1167. doi:https://doi.org/10.1016/j.clinph.2009.01.022

Lipsman, N., Sankar, T., Downar, J., Kennedy, S. H., Lozano, A. M., & Giacobbe, P. (2014). Neuromodulation for treatment-refractory major depressive disorder. *CMAJ : Canadian Medical Association journal = journal de l'Association medicale canadienne, 186*(1), 33-39. doi:10.1503/cmaj.121317

Liu, A., Vöröslakos, M., Kronberg, G., Henin, S., Krause, M. R., Huang, Y., . . . Buzsáki, G. (2018). Immediate neurophysiological effects of transcranial electrical stimulation. *Nature Communications, 9*(1), 5092. doi:10.1038/s41467-018-07233-7

Mehić, E., Xu, J. M., Caler, C. J., Coulson, N. K., Moritz, C. T., & Mourad, P. D. (2014). Increased anatomical specificity of neuromodulation via modulated focused ultrasound. *PLOS ONE, 9*(2), e86939-e86939. doi:10.1371/journal.pone.0086939

Miranda, P. C., Lomarev, M., & Hallett, M. (2006). Modeling the current distribution during transcranial direct current stimulation. *Clinical Neurophysiology, 117*(7), 1623-1629. doi:https://doi.org/10.1016/j.clinph.2006.04.009

Miyaguchi, S., Otsuru, N., Kojima, S., Saito, K., Inukai, Y., Masaki, M., & Onishi, H. (2018). Transcranial Alternating Current Stimulation With Gamma Oscillations Over the Primary Motor Cortex and Cerebellar Hemisphere Improved Visuomotor Performance. *Frontiers in behavioral neuroscience, 12*, 132-132. doi:10.3389/fnbeh.2018.00132

Miyaguchi, S., Otsuru, N., Kojima, S., Yokota, H., Saito, K., Inukai, Y., & Onishi, H. (2019). Gamma tACS over M1 and cerebellar hemisphere improves motor performance in a phase-specific manner. *Neuroscience Letters, 694*, 64-68. doi:https://doi.org/10.1016/j.neulet.2018.11.015

Moliadze, V., Antal, A., & Paulus, W. (2010). Electrode-distance dependent after-effects of transcranial direct and random noise stimulation with extracephalic reference electrodes. *Clinical Neurophysiology, 121*(12), 2165-2171. doi:https://doi.org/10.1016/j.clinph.2010.04.033

Moreines, J. L., McClintock, S. M., & Holtzheimer, P. E. (2011). Neuropsychologic effects of neuromodulation techniques for treatment-resistant depression: a review. *Brain stimulation, 4*(1), 17-27. doi:10.1016/j.brs.2010.01.005

Naro, A., Leo, A., Russo, M., Cannavò, A., Milardi, D., Bramanti, P., & Calabrò, R. S. (2016a). Does Transcranial Alternating Current Stimulation Induce Cerebellum Plasticity? Feasibility, Safety and Efficacy of a Novel Electrophysiological Approach. *Brain Stimulation: Basic, Translational, and Clinical Research in Neuromodulation, 9*(3), 388-395. doi:10.1016/j.brs.2016.02.005

Naro, A., Leo, A., Russo, M., Cannavò, A., Milardi, D., Bramanti, P., & Calabrò, R. S. (2016b). Does Transcranial Alternating Current Stimulation Induce Cerebellum Plasticity? Feasibility, Safety and Efficacy of a Novel Electrophysiological Approach. *Brain Stimulation, 9*(3), 388-395. doi:https://doi.org/10.1016/j.brs.2016.02.005

Newman, J. (1966). Resistance for Flow of Current to a Disk. *Journal of The Electrochemical Society, 113*(5), 501. doi:10.1149/1.2424003

Nitsche, M. A., Nitsche, M. S., Klein, C. C., Tergau, F., Rothwell, J. C., & Paulus, W. (2003). Level of action of cathodal DC polarisation induced inhibition of the human motor cortex. *Clinical Neurophysiology, 114*(4), 600-604. doi:https://doi.org/10.1016/S1388-2457(02)00412-1

Nitsche, M. A., & Paulus, W. (2000a). Excitability changes induced in the human motor cortex by weak transcranial direct current stimulation. *The Journal of physiology, 527 Pt 3*(Pt 3), 633-639. doi:10.1111/j.1469-7793.2000.t01-1-00633.x

Nitsche, M. A., & Paulus, W. (2000b). Excitability changes induced in the human motor cortex by weak transcranial direct current stimulation. *The Journal of physiology, 527*(3), 633-639. doi:10.1111/j.1469-7793.2000.t01-1-00633.x

Noetscher, G. M., Yanamadala, J., Makarov, S. N., & Pascual-Leone, A. (2014). Comparison of Cephalic and Extracephalic Montages for Transcranial Direct Current Stimulation—A Numerical Study. *IEEE Transactions on Biomedical Engineering, 61*(9), 2488-2498. doi:10.1109/TBME.2014.2322774

Oh, S.-J., Lee, J. M., Kim, H.-B., Lee, J., Han, S., Bae, J. Y., . . . Lee, C. J. (2019). Ultrasonic Neuromodulation via Astrocytic TRPA1. *Current Biology, 29*(20), 3386-3401.e3388. doi:10.1016/j.cub.2019.08.021

Opitz, A., Falchier, A., Yan, C.-G., Yeagle, E. M., Linn, G. S., Megevand, P., . . . Schroeder, C. E. (2016). Spatiotemporal structure of intracranial electric fields induced by transcranial electric stimulation in humans and nonhuman primates. *Scientific Reports, 6*(1), 31236. doi:10.1038/srep31236

Opitz, A., Paulus, W., Will, S., Antunes, A., & Thielscher, A. (2015). Determinants of the electric field during transcranial direct current stimulation. *NeuroImage, 109*, 140-150. doi:https://doi.org/10.1016/j.neuroimage.2015.01.033

Ozen, S., Sirota, A., Belluscio, M. A., Anastassiou, C. A., Stark, E., Koch, C., & Buzsáki, G. (2010). Transcranial Electric Stimulation Entrains Cortical Neuronal Populations in Rats. *The Journal of Neuroscience, 30*(34), 11476. doi:10.1523/JNEUROSCI.5252-09.2010

Parazzini, M., Rossi, E., Ferrucci, R., Liorni, I., Priori, A., & Ravazzani, P. (2014). Modelling the electric field and the current density generated by cerebellar transcranial DC stimulation in humans. *Clinical Neurophysiology, 125*(3), 577-584. doi:https://doi.org/10.1016/j.clinph.2013.09.039

Pelletier, S. J., & Cicchetti, F. (2014). Cellular and molecular mechanisms of action of transcranial direct current stimulation: evidence from in vitro and in vivo models. *The international journal of neuropsychopharmacology, 18*(2), pyu047. doi:10.1093/ijnp/pyu047

Person, A., & Raman, I. (2012). Synchrony and neural coding in cerebellar circuits. *Frontiers in Neural Circuits, 6*(97). doi:10.3389/fncir.2012.00097

Person, A. L., & Raman, I. M. (2011). Purkinje neuron synchrony elicits time-locked spiking in the cerebellar nuclei. *Nature, 481*(7382), 502-505. doi:10.1038/nature10732

Plaksin, M., Kimmel, E., & Shoham, S. (2016). Cell-Type-Selective Effects of Intramembrane Cavitation as a Unifying Theoretical Framework for Ultrasonic Neuromodulation. *eNeuro, 3*(3), ENEURO.0136-0115.2016. doi:10.1523/ENEURO.0136-15.2016

Plaksin, M., Shoham, S., & Kimmel, E. (2014). Intramembrane Cavitation as a Predictive Bio-Piezoelectric Mechanism for Ultrasonic Brain Stimulation. *Physical Review X, 4*(1), 011004. doi:10.1103/PhysRevX.4.011004

Pope, P., & Miall, R. (2014). Restoring Cognitive Functions Using Non-Invasive Brain Stimulation Techniques in Patients with Cerebellar Disorders. *Frontiers in Psychiatry, 5*(33). doi:10.3389/fpsyt.2014.00033

Pope, P. A., & Miall, R. C. (2012). Task-specific facilitation of cognition by cathodal transcranial direct current stimulation of the cerebellum. *Brain Stimulation, 5*(2), 84-94. doi:10.1016/j.brs.2012.03.006

Priori, A. (2003). Brain polarization in humans: a reappraisal of an old tool for prolonged non-invasive modulation of brain excitability. *Clinical Neurophysiology, 114*(4), 589-595. doi:https://doi.org/10.1016/S1388-2457(02)00437-6

Purpura, D. P., & McMurtry, J. G. (1965). Intracellular Activities And Evoked Potential Changes During Polarization Of Motor Cortex. *Journal of Neurophysiology, 28*(1), 166-185. doi:10.1152/jn.1965.28.1.166

Radman, T., Ramos, R. L., Brumberg, J. C., & Bikson, M. (2009a). Role of cortical cell type and morphology in subthreshold and suprathreshold uniform electric field stimulation in vitro. *Brain Stimulation, 2*(4), 215-228.e213. doi:https://doi.org/10.1016/j.brs.2009.03.007

Radman, T., Ramos, R. L., Brumberg, J. C., & Bikson, M. (2009b). Role of cortical cell type and morphology in subthreshold and suprathreshold uniform electric field stimulation in vitro. *Brain stimulation, 2*(4), 215-228.e2283. doi:10.1016/j.brs.2009.03.007

Rahman, A., Reato, D., Arlotti, M., Gasca, F., Datta, A., Parra, L. C., & Bikson, M. (2013). Cellular effects of acute direct current stimulation: somatic and synaptic terminal effects. *The Journal of physiology, 591*(10), 2563-2578. doi:10.1113/jphysiol.2012.247171

Rahman, A., Toshev, P. K., & Bikson, M. (2014). Polarizing cerebellar neurons with transcranial Direct Current Stimulation. *Clinical Neurophysiology, 125*(3), 435-438. doi:https://doi.org/10.1016/j.clinph.2013.10.003

Reato, D., Rahman, A., Bikson, M., & Parra, L. C. (2010). Low-intensity electrical stimulation affects network dynamics by modulating population rate and spike timing. *The Journal of neuroscience : the official journal of the Society for Neuroscience, 30*(45), 15067-15079. doi:10.1523/JNEUROSCI.2059-10.2010

Rezayat, E., & Toostani, I. G. (2016). A Review on Brain Stimulation Using Low Intensity Focused Ultrasound. *Basic and clinical neuroscience, 7*(3), 187-194. doi:10.15412/J.BCN.03070303

Roche, N., Geiger, M., & Bussel, B. (2015). Mechanisms underlying transcranial direct current stimulation in rehabilitation. *Annals of Physical and Rehabilitation Medicine, 58*(4), 214-219. doi:https://doi.org/10.1016/j.rehab.2015.04.009

Ruffini, G., Wendling, F., Merlet, I., Molaee-Ardekani, B., Mekonnen, A., Salvador, R., . . . Miranda, P. C. (2013). Transcranial Current Brain Stimulation (tCS): Models and Technologies. *IEEE Transactions on Neural Systems and Rehabilitation Engineering, 21*(3), 333-345. doi:10.1109/TNSRE.2012.2200046

Schmahmann, J. D. (2004). Disorders of the Cerebellum: Ataxia, Dysmetria of Thought, and the Cerebellar Cognitive Affective Syndrome. *The Journal of Neuropsychiatry and Clinical Neurosciences, 16*(3), 367-378. doi:10.1176/jnp.16.3.367

Schutter, D. J. L. G., & Wischnewski, M. (2016). A meta-analytic study of exogenous oscillatory electric potentials in neuroenhancement. *Neuropsychologia, 86*, 110-118. doi:https://doi.org/10.1016/j.neuropsychologia.2016.04.011

Schweid, L., Rushmore, R. J., & Valero-Cabré, A. (2008). Cathodal transcranial direct current stimulation on posterior parietal cortex disrupts visuo-spatial processing in the contralateral visual field. *Experimental Brain Research, 186*(3), 409-417. doi:10.1007/s00221-007-1245-0

Shah, B., Nguyen, T. T., & Madhavan, S. (2013). Polarity Independent Effects of Cerebellar tDCS on Short Term Ankle Visuomotor Learning. *Brain Stimulation, 6*(6), 966-968. doi:https://doi.org/10.1016/j.brs.2013.04.008

Smitt, J. W., & Wegener, C. F. (1944). ON ELECTRIC CONVULSIVE THERAPY. *Acta Psychiatrica Scandinavica, 19*(3-4), 529-549. doi:10.1111/j.1600-0447.1944.tb04586.x

Stagg, C. J., Best, J. G., Stephenson, M. C., O'Shea, J., Wylezinska, M., Kincses, Z. T., . . . Johansen-Berg, H. (2009). Polarity-sensitive modulation of cortical neurotransmitters by transcranial stimulation. *The Journal of neuroscience : the official journal of the Society for Neuroscience, 29*(16), 5202-5206. doi:10.1523/JNEUROSCI.4432-08.2009

Stagg, C. J., Best, J. G., Stephenson, M. C., Shea, J., Wylezinska, M., Kincses, Z. T., . . . Johansen-Berg, H. (2009). Polarity-Sensitive Modulation of Cortical Neurotransmitters by Transcranial Stimulation. *The Journal of Neuroscience, 29*(16), 5202. doi:10.1523/JNEUROSCI.4432-08.2009

Tanaka, T., Takano, Y., Tanaka, S., Hironaka, N., Kobayashi, K., Hanakawa, T., . . . Honda, M. (2013). Transcranial direct-current stimulation increases extracellular dopamine levels in the rat striatum. *Frontiers in Systems Neuroscience, 7*(6). doi:10.3389/fnsys.2013.00006

Tang, T., Blenkinsop, T. A., & Lang, E. J. (2019). Complex spike synchrony dependent modulation of rat deep cerebellar nuclear activity. *eLife, 8*, e40101. doi:10.7554/eLife.40101

Tang, T., Suh, C. Y., Blenkinsop, T. A., & Lang, E. J. (2016). Synchrony is Key: Complex Spike Inhibition of the Deep Cerebellar Nuclei. *Cerebellum (London, England), 15*(1), 10-13. doi:10.1007/s12311-015-0743-z

ter Haar, G. (1999). Therapeutic ultrasound. *European Journal of Ultrasound, 9*(1), 3-9. doi:https://doi.org/10.1016/S0929-8266(99)00013-0

Terzuolo, C. A., & Bullock, T. H. (1956). MEASUREMENT OF IMPOSED VOLTAGE GRADIENT ADEQUATE TO MODULATE NEURONAL FIRING. *Proceedings of the National Academy of Sciences, 42*(9), 687. doi:10.1073/pnas.42.9.687

Tufail, Y., Matyushov, A., Baldwin, N., Tauchmann, M. L., Georges, J., Yoshihiro, A., . . . Tyler, W. J. (2010). Transcranial Pulsed Ultrasound Stimulates Intact Brain Circuits. *Neuron, 66*(5), 681-694.doi:https://doi.org/10.1016/j.neuron.2010.05.008

Tyler, W. J. (2012). The mechanobiology of brain function. *Nature Reviews Neuroscience, 13*(12), 867-878. doi:10.1038/nrn3383

Tyler, W. J., Tufail, Y., Finsterwald, M., Tauchmann, M. L., Olson, E. J., & Majestic, C. (2008a). Remote excitation of neuronal circuits using low-intensity, low-frequency ultrasound. *PLOS ONE, 3*(10), e3511-e3511. doi:10.1371/journal.pone.0003511

Tyler, W. J., Tufail, Y., Finsterwald, M., Tauchmann, M. L., Olson, E. J., & Majestic, C. (2008b). Remote Excitation of Neuronal Circuits Using Low-Intensity, Low-Frequency Ultrasound. *PLOS ONE, 3*(10), e3511. doi:10.1371/journal.pone.0003511

Van Dijck, G., Van Hulle, M. M., Heiney, S. A., Blazquez, P. M., Meng, H., Angelaki, D. E., . . . Holtzman, T. (2013). Probabilistic Identification of Cerebellar Cortical Neurones across Species. *PLOS ONE, 8*(3), e57669. doi:10.1371/journal.pone.0057669

Van Overwalle, F., Baetens, K., Mariën, P., & Vandekerckhove, M. (2014). Social cognition and the cerebellum: A meta-analysis of over 350 fMRI studies. *NeuroImage, 86*, 554-572. doi:https://doi.org/10.1016/j.neuroimage.2013.09.033

Vöröslakos, M., Takeuchi, Y., Brinyiczki, K., Zombori, T., Oliva, A., Fernández-Ruiz, A., . . . Berényi, A. (2018). Direct effects of transcranial electric stimulation on brain circuits in rats and humans. *Nature Communications, 9*(1), 483. doi:10.1038/s41467-018-02928-3

Vossen, A., Gross, J., & Thut, G. (2015). Alpha Power Increase After Transcranial Alternating Current Stimulation at Alpha Frequency (α-tACS) Reflects Plastic Changes Rather Than Entrainment. *Brain stimulation, 8*(3), 499-508. doi:10.1016/j.brs.2014.12.004

Watson, T., Becker, N., Apps, R., & Jones, M. (2014). Back to front: cerebellar connections and interactions with the prefrontal cortex. *Frontiers in Systems Neuroscience, 8*(4). doi:10.3389/fnsys.2014.00004

Wiley, J. D., & Webster, J. G. (1982). Analysis and Control of the Current Distribution under Circular Dispersive Electrodes. *IEEE Transactions on Biomedical Engineering, BME-29*(5), 381-385. doi:10.1109/TBME.1982.324910

Woods, A. J., Antal, A., Bikson, M., Boggio, P. S., Brunoni, A. R., Celnik, P., . . . Nitsche, M. A. (2016). A technical guide to tDCS, and related non-invasive brain stimulation tools. *Clinical Neurophysiology, 127*(2), 1031-1048. doi:https://doi.org/10.1016/j.clinph.2015.11.012

Yamaguchi, S., Tsuchiya, H., & Kobayashi, S. (1998). Visuospatial Attention Shift and Motor Responses in Cerebellar Disorders. *Journal of Cognitive Neuroscience, 10*(1), 95-107. doi:10.1162/089892998563806

Yoo, S.-S., Bystritsky, A., Lee, J.-H., Zhang, Y., Fischer, K., Min, B.-K., . . . Jolesz, F. A. (2011). Focused ultrasound modulates region-specific brain activity. *NeuroImage, 56*(3), 1267-1275. doi:10.1016/j.neuroimage.2011.02.058

Yuan, Y., Yan, J., Ma, Z., & Li, X. (2016). Noninvasive Focused Ultrasound Stimulation Can Modulate Phase-Amplitude Coupling between Neuronal Oscillations in the Rat Hippocampus. *Frontiers in Neuroscience, 10*(348). doi:10.3389/fnins.2016.00348

Zaehle, T., Rach, S., & Herrmann, C. S. (2010). Transcranial Alternating Current Stimulation Enhances Individual Alpha Activity in Human EEG. *PLOS ONE, 5*(11), e13766. doi:10.1371/journal.pone.0013766